A report for the

Commonwealth Department of Climate Change and Energy Efficiency (DCCEE)

April 2011

Editor: John Ginger, Cyclone Testing Station

Task 1: Bob Cechet, Augusto Sanabria, Geoscience Australia

Task 2: Jeff Kepert, Bureau of Meteorology; John Holmes, JDH Consulting

Task 3: John Ginger, David Henderson, Cyclone Testing Station, James Cook University

Extreme Windspeed Baseline Climate Investigation Project

misleading, as it was based on an earlier definition of the averaging time of the gust recorded by

ACKNOWLEDGEMENTS

The Extreme Windspeed Baseline Investigation Project is a collaboration between the Cyclone Testing Station at James Cook University, the Bureau of Meteorology, John Holmes Consulting and Geoscience Australia. The authors gratefully acknowledge the financial support from the Department of Climate Change and Energy Efficiency (DCCEE) and the Australasian Wind Engineering Society (AWES) and the Bureau of Meteorology for the support and valued assistance.

The authors would like to thank;

Jim Davidson, Director, Bureau of Meteorology, Queensland
Doug Fraser and Mats Einerman, Bureau of Meteorology, Townsville
Dave Edwards, Paul Leigh and Jim Easson, Bureau of Meteorology, Melbourne
Ian Muirhead, Bureau of Meteorology, National Climate Centre, Melbourne
Sean Carson, Bureau of Meteorology, Canberra
Murray Morrison, University of Western Ontario
Rachael Dempsey (now Murray Darling Basin Authority)

Extreme Windspeed Baseline Climate Investigation Project

TABLE OF CONTENTS

EXECUTIVE SUMMARY …….. 3
Outcomes of the project **5**
Recommendations of the project **5**
ACKNOWLEDGEMENTS ……. 7
INTRODUCTION …… 9
OVERVIEW …… 9
TASK 1: Statistical comparison of historical daily gust data from those cases where

INTRODUCTION

This project aims to establish the response characteristics of the now obsolete Dines Anemometer and the Synchrotac 3-cup anemometers currently used by the Bureau of Meteorology. Three types of Dines anemometers (mainly high speed in cyclone areas and low-speed in non-cyclone areas, plus a few intermediate speed instruments) were used at a number of sites in Australia, and these have been progressively replaced by 3-cup anemometers commencing in the mid 1980s. In addition, new sites have been added to the network by the Bureau of Meteorology. The Bureau of Meteorology advises that at a number of sites, the cup and Dines instruments have collected data in parallel, notwithstanding that only the data from one instrument may be in the official data record (Metadata). Both instruments are still operational at a few sites. Hence, wind speed data from each instrument at

a)

TASK 1: STATISTICAL COMPARISON OF HISTORICAL DAILY GUST DATA FROM THOSE CASES WHERE THE TWO ANEMOMETER SYSTEMS WERE OPERATING IN PARALLEL

This task sought to examine the observed record of peak gust wind speed (daily maximum gust wind speed) in order to establish the existence of a bias between the early part of the record (obtained using pressure-tube Dines anemometers) and the later part of the record (obtained using 3-cup anemometers). All observational data as well as metadata was obtained from the Bureau of Meteorology. The 38 recording stations considered were all situated at airports and were in the most part staffed by Bureau of Meteorology officers. To isolate the issue of anemometer replacement (i.e. reduce concerns regarding consistent instrument exposure), only observing stations located at airports and with more than 30 years of record were considered.

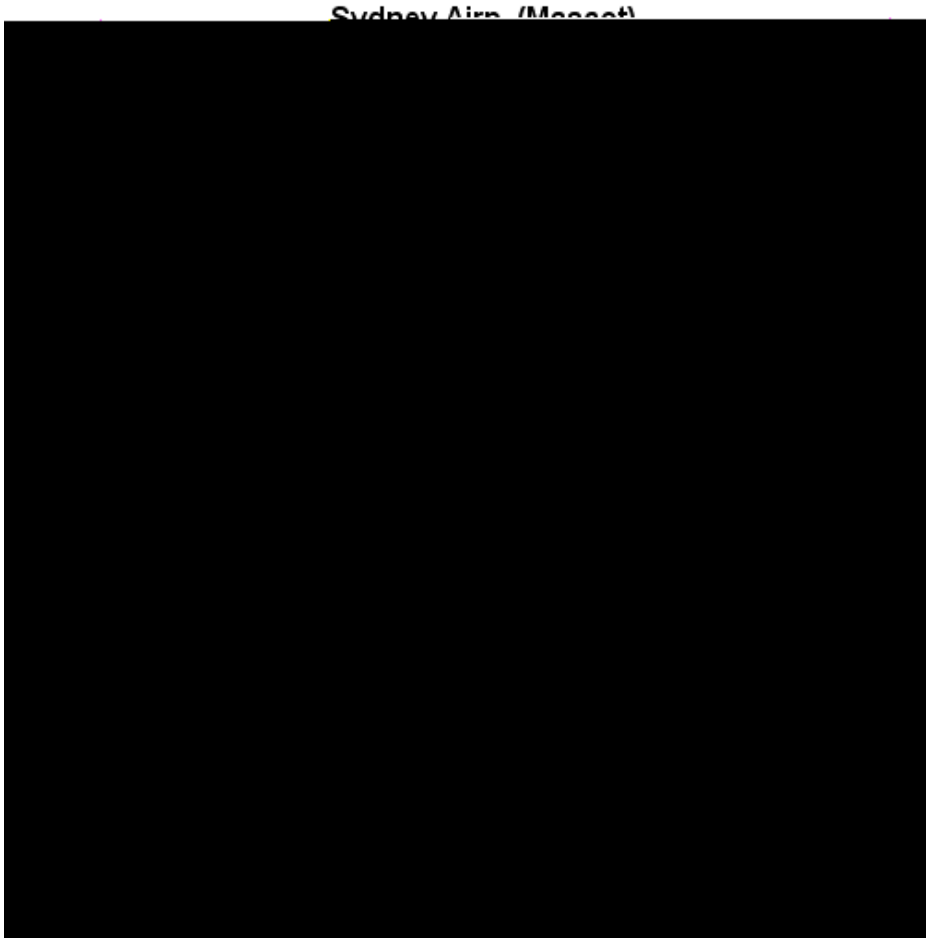

Figure 1-1. Time-series plots of the daily maximum gust wind speed (above a threshold of 25 m/s) for the Sydney, Melbourne and Adelaide (airport) meteorological observing station. The broken vertical line indicates the replacement of the Dines anemometer with a 3-cup anemometer.

The visual inspection of the observed daily peak gust wind speed time-series for most of the Bureau of Meteorology observing sites considered in this study is sufficient to indicate that in general

minute intervals); this increases to about 12 to 17% higher at gust wind speeds around 60 m/s. These systematic differences are consistent with those reported by Reardon *et al*. (1999) and Reardon (2000), and confirm concerns about the consistency of the peak gust wind speed observational database which underpins the Australian wind loading standard (AS/NZS 1170.2, 2010).

Figure1-2. Return period plots of coincident maximum gust wind speed (above a threshold of 15 m/s for 30 minute time sections) for the combined 7 northern Australian observing stations over a total coincident measurement period of 89 years. 95% confidence limits for the GPD fit to the Dines anemometer observations are also provided.

Table 1-1. Percentage difference (return period gust wind speed) between the Dines anemometer and cup anemometers over a range of wind speeds, considering coincident extreme wind gust measurements at 7 observing sites over a total coincident measurement period of 89 years. The asymptotic nature of the GPD fit to the observations does not allow a comparison for gust wind speeds above 60 m/s.

Cup anemometer gust wind speed	Dines anemometer gust wind speed	Dines; Lower 95% confidence limit	Dines; Upper 95% confidence limit

Recommendation from Task 1

- This analysis allows the calculation of factors which will provide corrections to be made to daily maximum gust wind speed data in order to obtain a uniform record. It appears that a significantly lower amplitude wind gust is currently being recorded by the Bureau of Meteorology (BoM). This is chiefly the result of a decision of the BoM (based on W.M.O. advice) to apply a 3-second moving average filter to the 3-cup Synchrotac anemometer recorded daily gusts (see further explanation later in the report). It is recommended that experimental evidence detailing the impact of the "digital filtering" on the

TASK 2: REVIEW OF PREVIOUS STUDIES OF RESPONSE CHARACTERISTICS OF THE DINES

(c) Statistical comparison of peak velocities recorded by Dines, cup and sonic anemometers using time histories

In this Sub-Task, using time histories of Dines float movement generated experimentally in Task 3, a statistical comparison of peak velocities recorded by the Dines anemometer a 3-cup anemometer and a sonic anemometer was made. This was achieved by processing of a time series of wind velocity which was used to drive the float system of a low-speed Dines anemometer.

This work indicated that the Dines anemometer under-estimated the „true" peaks that would have been recorded by a sonic anemometer by 5-10%, but over-predicted the peaks recorded by the cup anemometer by 2-5%. This work is discussed in detail in the Appendix II-3.

However, in order to derive appropriate correction factors for past recordings of daily gusts in Australia, it is necessary to account for the 3-second moving average filter applied in the Automatic Weather Stations by the Bureau of Meteorology in accordance with the WMO standard. This aspect was investigated in another Sub-Task, described following.

oscillation in the water and of the float are given by equations 22 to 25 of Appendix II-5. These frequencies depend upon several factors, including the mean wind speed. These oscillations have been noted in a few of the historical laboratory test reports, notably Borges (1968), but have not been previously analysed mathematically.

Numerical solutions were obtained using a fourth-order Runge-Kutta scheme, with a sample simulation is shown here as Figure 2.1. In this sample, both the in-phase and out-of-phase oscillations are clearly present, with a periodic transfer of energy between the two.

In reality, Dines anemometers possess several sources of friction, which acts to damp the motion of the float and water. These dampings include of the float directly (due e.g. to friction of the pen arm), and of the water directly (due to friction between the water and the tank). However, the most significant damping is believed to be due to the passage of water in and out of the float bottom, where a “choke”, shown in Figure 15 of Appendix II-5, significantly impedes the flow. All three sources of damping are represented in the equations derived to model the system as first-order linear dampings characterised by individual time constants (see equations 1 to 5 of Appendix II-5).

The solution to the forced damped equations depends on the relationship between the forcing, strength of the damping, and the resonant frequencies. Forcing near the resonance produces the strongest response. The amplitude of the response can vary from zero to several times the amplitude of the forcing, depending on the degree of the damping and the frequency of the forcing.

Response curves are shown for a sample configuration in Figure 2-2. These curves show the relative amplitude and phase of the oscillation as a function of forcing frequency, with the blue curve representing the float and the green, the water. The amplitudes have been scaled by the forcing amplitude, so that amplitude=1, phase=0 means the float exactly follows the varying wind speed. The magenta diamonds indicate the linear undamped frequencies, and are clearly close to the resonant peaks. At low frequencies, the float closely follows the wind speed, with a rising response to the out-of-phase oscillation near the lower resonant frequency, and a second weaker peak near the higher resonance, with a weak trough between. The phase response shifts from in-phase at low frequencies, to out-of-phase at high.

The dual peak in the response curve significantly complicates attempts to calculate the “gust period” or “response time” that the Dines anemometer measures. Such calculations are straightforward for the more usual first-order systems, but not for those one, let alone two, significant resonances. Accordingly, due care is urged in interpreting such calculations.

Figure 2-2 is in very good agreement with the measurements of Borges (1968). Figure 2-3 reproduces a similar curve (of the float motion only) from his laboratory experiments, showing good quantitative agreement with the model. Both the amplitude and phase of the response are well represented (some tuning of the damping in the model was necessary to achieve this good agreement). The results in Figure 2-3 are similarly in good agreement with the measurements taken by the CTS as part of Task 3 of this project, although here the agreement is more qualitative than quantitative as the higher-frequency peak is stronger. Close agreement with the Dines measurements is possible with re-tuning of the physical constants in the model equations, implying that the Fuess anemometer used by Borges has some significant differences from the Dines anemometer.

The second model removes the simplifications to the geometry made in the above model and is described in section 2 of Appendix II-5. Figure 2-4 summarises the behaviour of the system, configured to model a low-speed Dines anemometer, in the absence of damping. As for the U-tube analogue, there are two dominant resonant frequencies, with the water moving in- or out-of-phase with the float. The figure shows that the lower-frequency oscillation, in which the float and water

inside it move in phase, has a frequency of 0.49 Hz at a mean wind speed of 10 m/s which increases slowly with wind speed to 0.75 Hz at 50 m/s. The higher-frequency, out-of-phase motion, has a frequency that increases from about 1 to 3 Hz as the mean wind speed increases from 10 to 50 m s^{-1}. At a mean wind speed of 20 m s^{-1}, similar to that of the laboratory measurements conducted by the Cyclone Testing Station, the two frequencies are about 0.55 Hz and 1.45 Hz, within about 0.1 Hz of the measured resonant frequencies. This is excellent agreement; the small discrepancy is probably due to some simplifying assumptions in the model, the difficulty of measuring the response frequencies to high precision in the laboratory, that damping may slightly shift the frequencies, and experimental uncertainty in the measured resonant frequencies. As with the first model, there are also weaker spectral peaks at harmonics and interharmonics of the dominant resonances.

The strong agreement with the laboratory measurements provides considerable confidence in the model. There is no tuning of these results, they were obtained simply by inserting the correct float geometry and mass and chamber geometry into the equations. Calibration of the second model would be assisted by detailed drawings and specifications of the float and chamber, particularly for the rarer 150 and 200 m.p.h. models of the instrument. The former manufacturer of the Dines anemometer, R.M. Munro, very kindly agreed to search their archives for such drawings, unfortunately without success.

In the absence of firm information, a hypothetical configuration of the model for a high-speed instrument was attempted. This utilised some measurements of the outside of the tank, together with reasonable estimates of the float characteristics, as detailed in Appendix II-5. Compared to the low-speed instrument, the dominant oscillation shifts to a lower frequency, about 0.3 Hz with a weak increase at higher wind speeds, while the higher-frequency oscillation increases in frequency. The reduction in frequency of the in-phase oscillation is in good agreement with the laboratory measurements and is consistent with the approximate doubling of the oscillating mass. However, the increase in frequency of the out-of-phase oscillation seems somewhat larger than found in the laboratory measurements. However, until firm information on the physical characteristics of the high-speed float become available, the cause for this discrepancy cannot be determined.

This sensitivity of the results to the physical characteristics of the instrument implies that care will be needed in interpreting the results of this study to ensure that the appropriate model of Dines

Figure 2- 1. Time-series of unforced, undamped numerical solutions to the full nonlinear equations for the simplified model. The upper panel shows the float (blue) and water (green) positions, and the lower panel their velocities. The thin curves show the instantaneous positions and velocities, both in-phase and out-of-phase oscillations are clearly present. In the top panel, the thick blue curve shows the low-pass filtered float position, showing the long-period oscillation due to a nonlinear interaction between the in-phase and out-of-phase oscillations. The thick blue line the mean position for that wind speed with no fluctuations, and the thin dashed line is the actual mean float position. The difference between these curves indicates that the instrument is “overspeeding”.

Figure 2-4. Logarithm base-10 of the power spectral density of the position of the float (top), water level in the tank (middle), and water level inside the float (bottom), as a function of the mean wind

- The application of a 3-second moving average filter to the cup anemometer outputs in the Automatic Weather Stations (AWS) by the BoM in accordance with international practice has resulted in a further increase in the *apparent* average overshoot of the Dines anemometers to 7-13% for the low-speed type, and to 12-21% for the high-speed type.
- The 3-second moving average in the AWSs has led to „double-filtering‟ of the wind turbulence. It has resulted in a „mismatch‟ between the definition of maximum gust used for design for wind loading in Australia since 1971. However, we note that this averaging follows the recommended procedure by the World Meteorological Organisation, and is consistent with international practice. In principle, it should be possible to adjust gusts measured under this averaging to other averaging periods, or to no averaging, provided that the relevant anemometer characteristics are known.

Recommendations from Task 2

- The definition of peak gust used in the Australian/New Zealand Standard for wind actions should be reviewed by Standards Australia, since a significantly lower gust is currently being recorded by the Bureau of Meteorology (BoM). The latter has resulted from the decision of the BoM to apply a 3-second moving average filter applied in the Automatic Weather Stations to recorded daily gusts in Australia.
- Factors have been derived to allow corrections to be made to daily maximum gusts formerly generated by the Dines anemometers (both low-speed and high-speed types), and currently being generated by Automatic Weather Stations in Australia. These correction factors should be applied before extreme value analyses are undertaken to develop revised design wind speeds for structures.

References for Task 2

A.R.J. Borges, 1968: On the frequency response of floater-type anemographs, Tecnica, No. 379, pp505-511.

J.J. Logue, 1986: Comparison of wind speeds recorded simultaneously by a pressure-tube anemograph and a cup-generator anemograph. *Met. Mag.*, **115,** pp 178-185.

TASK 3: EXPERIMENTAL TESTING OF THE DINES PRESSURE TUBE AND FLOAT FOR DYNAMIC CHARACTERISTICS USING A RAPID PRESSURE LOADING ACTUATOR (PLA).

Introduction

The response of low-speed and high-speed Dines instruments were studied by testing these, as part of Task 3 of the project. The objectives were to measure the response of the Low Speed and High Speed Dines float when excited by a known pressure signal applied to the head. Various pressure signals with differing frequencies and amplitudes were generated using a Pressure Loading Actuator (PLA) capable of applying rapidly fluctuating realistic wind pressures.

Figures 3-1 to 3-3 show the high speed Dines anemometer tower at the site, and the float chamber with paper record drum float rod and recorder. The Dines anemometer in Townsville was replaced by the 3-cup Synchrotac anemometer and direction vane, as the official wind speed measurement device in the early 1990s. Figure 3-4 shows the Bureau of Meteorology 3-cup anemometer at the Townsville Airport. However, the Dines has been kept operational as an unofficial wind speed recording device to-date, as noted by Reardon *et al* (1999). This provides an opportunity to compare the "performance" of both instruments which are located about 100m apart, at Townsville Airport,.

A low-speed Dines anemometer, including the head and vane, float and chamber, from Glenlitta Victoria was loaned to the CTS by the Bureau of Meteorology. The low-speed units were typically used in non-cyclonic regions (and in cyclonic regions prior to the mid-70s). This system was set-up in the laboratory at the CTS and series of experiments were conducted prior to testing the high-speed system at the Airport in Townsville. This enabled any potential difficulties to be identified and rectified in controlled lab conditions before conducting tests in the field.

Tests were carried out on these two instruments over a period of about five months in 2010. Details of these tests and results are provided in Appendix III of this report. The focus of these tests were to ascertain the response of these two Dines instruments, and provide test results to Task 2 for calibration and validation of the mathematical models. The analysis carried out in Task 1 is also assessed against these test results.

Experiments and Data Collection

Recent development of the advanced Pressure Loading Actuator (PLA) that can simulate

Figure 3-1 Dines anemometer

Figure 3-2. High Speed Float Chamber

Figure 3-3. Float rod and speed recorder

Figure 3-4. 3-cup anemometer

Pressure input to the Dines and Dines output

pressure transducers located in the manifold immediately in front of the inlet of the Dines head. One pressure transducer (PT) was used by the PLA for controlling the valve to achieve the requested pressure trace. The second PT output was recorded using the same data acquisition (DAQ) module that recorded the response of the LVDT attached to the float. The DAQ used a simultaneous sampling system ensuring that the input and output (i.e. PT and LVDT measurements) were synchronized.

The output of the Dines float chamber is measured by the vertical rise and fall of a float rod attached to the top of the float chamber. The vertical movement is typically transcribed directly onto a

Test configurations

A range of test configurations were set-up to examine the contribution of each component of the Dines systems to the overall frequency respon

pressure trace was applied to the systems. The vertical displacement of the float rod measured by the LVDT (in mm) was recorded vs Δp and converted to an equivalent velocity using Equation 3-1. Figures 3.7 and 3.8 show the measured response of the low- and high-speed Dines float chambers respectively, obtained by applying the "static" pressure traces. The linear relationship between the velocity, and the low- and high-speed Dines responses are 0.29 and 0.59 ms^{-1}/mm, respectively. The vertical axis (wind speed) of the actual Dines paper chart measured 177 mm for the maximum speed of 100 and 200 knots, thus each mm on the standard and high speed charts is equivalent to 0.290 and 0.583 m/s. Following calibration of the float rod with the LVDT, the vertical movement of the float rod was>>BDC -43p >>Bp91(t26 -15 0 Td9)6(nd)-53(sp)9(ee)--43p5n(ee)--43p5n(ee)--4cocidp1ID 26 -133-o-75( )T

The Low-Speed and High Speed Dines instruments were subjected to a range of input fluctuating pressures derived from wind speeds measured by a sonic anemometer and in a wind tunnel. The mean wind speeds were 20, 25 and 30 m/s for the Low speed Dines and higher than 50 m/s for the High Speed Dines. The turbulence intensities varied from ~10 to 20%. Figure 3-9 shows a portion of the Sonic anemometer input and Low Speed Dines response for a mean velocity of 25 m/s and turbulence intensity of 10%. The Dines "follows" the wind speed time trace. The mean wind speed is

Australian extreme windspeed baseline climate investigation project

APPENDIX I.

Intercomparison of time-series and coincident

Dines & cup anemometer observations.

NOTE: This report is to be published as a Geoscience Australia Record

GA Record 2011/xx:

by R.P. Cechet[1] and L.A. Sanabria[1]

1. Risk and Impact Analysis Group, Geoscience Australia

Dines anemometer (image supplied by Cyclone Testing Station, James Cook University)

Coincident Dines & cup anemometer observations

Coincident gust wind speed measurements at 7 northern Australian observing stations were analysed to determine the magnitude of the direct bias. Only Dines "high-speed range" anemometers (0-200 knots) were considered for observing stations where extreme wind gusts are dominated by thunderstorm and tropical cyclone events. The stations examined were Cairns, Townsville, Brisbane, Darwin, Gove, Broome and Learmonth. Coincident probability distributions (PDF's) of the gust wind speed ((Dines & cup anemometer) for the seven sites display systematic bias with regards to the peak of the distribution for some of the observing stations. The peak of the Dines anemometer PDF appears slightly low for Darwin and too high for Learmonth and Townsville in comparison to the cup anemometer. Agreement is excellent for Cairns. In general, the time-series plots of the bias between the Dines and cup anemometer measurements show no time dependent relationships.

The data on the extreme gust wind speeds for the 7 sites (total perio16(e)1(de)1gards to

Appendix I - A. 45
Scatterplots of the gust wind speed datasets

Appendix I - B. 53
Return period (RP) plots of gust wind speed for the 31 “Region A” observing stations considered in Sections 4.1 & 4.2 (see Figure 6 for observing station locations depicted on a map of Australia).

Appendix I - C. 61
Coincident Dines and cup anemometer observations
(i) Probability distributions of gust wind speeds
(ii) Bias between coincident Dines and cup anemometer observations

To provide a benchmark measure of severe wind hazard nationally (current climate), this study has investigated the

- consistency of the time-series observations of extreme wind speed;
- comparison of coincident observations from the "old" and "new" types of observing instruments.

1.2. BACKGROUND

The Australian Government, through the Australian Building Codes Board (ABCB), has responsibility for maintenance of the Building Code of Australia (BCA). The BCA establishes performance requirements that buildings must satisfy when subjected to the actions of, among other hazards, severe winds. In relation to wind actions, the BCA references two Standards to establish the performance requirements – AS/NZS 1170.2:2002 *Structural design actions Part 2; Wind actions* and AS 4055:2006 *Wind loads for housing*. In each State and Territory, the BCA forms part of the building regulations, enforced through legislation at that level.

The visual inspection of the observed daily peak gust wind speed time-series for most of the Bureau of Meteorology observing sites considered in this study is sufficient to indicate that in general *"the early part of the record contains a higher frequency of extreme events, and also the largest amplitude extreme events"*. Figure 2 shows time-series plots of the daily maximum gust wind speed (above a threshold of 25 m/s) for the Sydney, Melbourne and Adelaide meteorological observing stations. Visual inspection indicates that the early part of the record (Dines anemometer) contains a greater number and also higher amplitude extreme events compared to the later part of the record (replacement cup anemometer). Time-series plots of gust wind speed for all stations considered are shown in Appendix I-A.

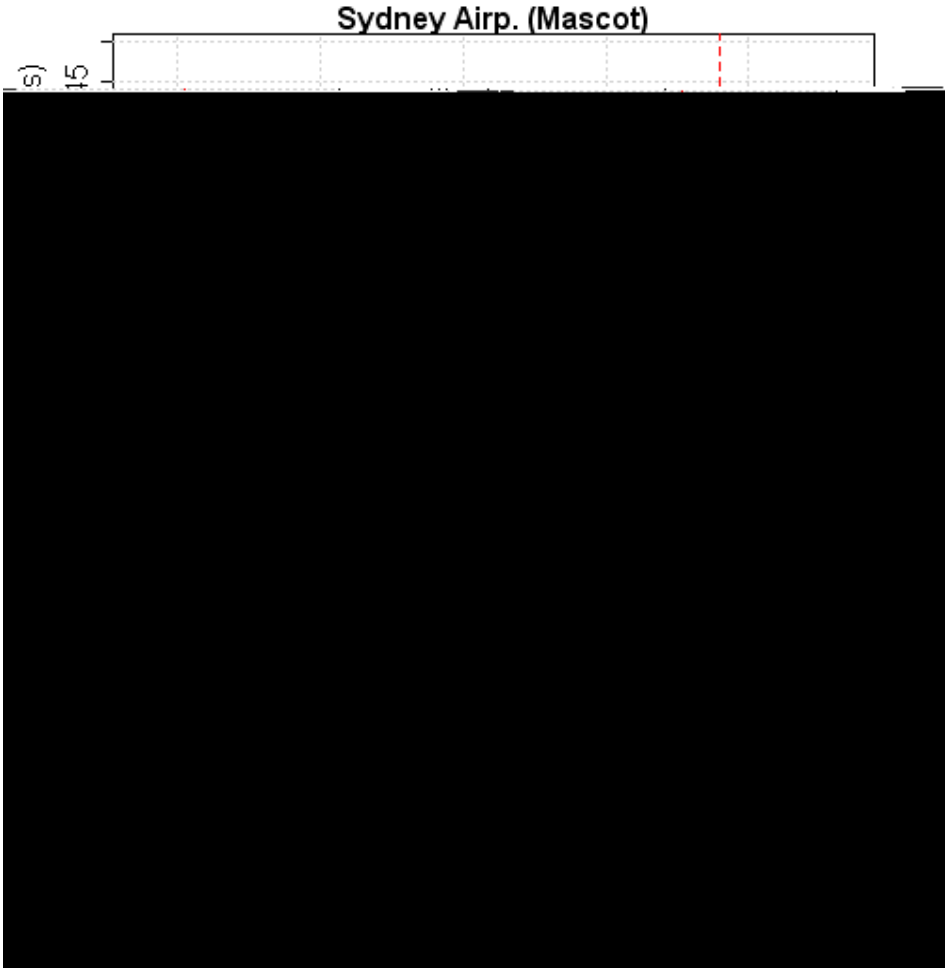

Fig. 2. Time-series plots of the daily maximum gust wind speed (above a threshold of 25 m/s) for the Sydney, Melbourne and Adelaide (airport) meteorological observing station. The broken vertical line indicates the replacement of the Dines anemometer with a cup anemometer.

The installation of the pressure-tube (Dines) anemometer (described in Jacobson, 2005; Knowles

2. Methodology

2.1. STATISTICAL MODEL

The results presented here were generated using a statistical model of severe winds developed by Geoscience Australia (Sanabria & Cechet, 2007). Although statistical models have limitations, they are useful for the assessment of potential severe winds at discrete points in a region and are fundamental for the calculation of hazard from records of observational gust wind speed datasets. Statistical methods are extensively utilised in the current Australian wind loadings standard (AS/NZS 1170.2, 2002).

The main limitation of statistical models is their dependency on the quality of the observational data

These parameters must satisfy; $-\infty < \mu < \infty$, $\sigma > 0$, and $-\infty < \xi < \infty$, and the value of the shape parameter defines which specific distribution is being fitted to the given data:,

- If $\xi < 0$, a GEV type III or ***Weibull*** distribution is used. This distribution has a convex (bounded) curve.

- If $\xi > 0$, a GEV type II or ***Frechet*** distribution is used. This distribution has a concave (unbounded) curve.

- If $\xi = 0$, a GEV type I or ***Gumbel*** distribution which is a straight line, is used.

A number of techniques to fit these distributions to the given data have been developed. The most effective are the maximum likelihood and the method of moments. Figure 3 shows the Sydney airport data fitted using seven different techniques: maximum likelihood (mle), method of moments (moments), unbiased probability weighted moments (pwmu), biased probability weighted moments (pwmb), minimum density power divergence (mdpd), medians (med) and likelihood moment (lme). Although in most cases they give similar results, other examples (not presented here) show that the most effective technique to fit GEV distributions to wind speed datasets is the 'mle' method. Palutikoff et al., (1999) and Seguro and Lambert (2000) report similar results; for this reason the 'mle' technique will be used throughout this work.

Figure 3. Fitting the GEV to gust wind speeds using a number of techniques.

2.3. GENERALISED PARETO DISTRIBUTION (GPD)

Applying the methods to temperature data, Gillelland and Katz found out that the Profile-likelihood method gives better results because it considers the asymmetry of the data (Gilleland and Katz 2005b). Figure 4 shows the RP of the Sydney Airport combined winds (black line) with 95%

2.4. R- PROGRAMMING ENVIRONMENT

The software utilised for this study was developed using the R-programming environment on a computer running the Linux operating system. One of the main advantages of R is the large collection of specific-purpose packages developed by the user community. For this project extensive use of R-programming environment packages for extreme value analysis were used (Stephenson 2004; Gilleland and Katz, 2005a).

The methodology used in this study can be summarised in the following steps:

- Select a particular wind recording station with available maximum daily wind speed and weather description datasets,
- Merge the wind dataset with the corresponding weather description dataset,
- From the merged dataset, extract thunderstorm wind speeds and construct a thunderstorm wind dataset. The remainder of the original dataset is termed the synoptic wind dataset. The

3. Data

This study has examined the observed record of **peak gust wind speed** (daily maximum gust wind speed) in order to establish the existence of a bias between the early part of the record (obtained using pressure-tube Dines anemometers) and the later part of the record (obtained using cup anemometers). All observational data (38 observing stations considered) as well as all the metadata was obtained from the Bureau of Meteorology. All recording stations considered were situated at airports which were in the most part staffed by Bureau of Meteorology officers. To isolate the issue of anemometer replacement, only observing stations located at airports (consistent exposure) and with more than 30 years of record were considered.

3.1 GUST WIND SPEED DATA

All wind datasets used in this study were acquired by GA from the Australian Bureau of Meteorology (BoM). The wind speed data contains six types of datasets from 134 recording stations (not all types available for all stations):

- `1min'. - contain one-minute averaged wind speed records,
- `3hour'. - contain three-hourly observations of wind speed (10 minute average),
- `hhourly'. - contain half-hourly observations of wind speed (10 minute average), and
- `MxDai'. - contain maximum daily gust wind speed records.
- `weatherd'. - contain 3-hourly weather description records,
- `metadata'. - contain a comprehensive description of wind station characteristics and an explanation of the type of data recorded by the station.

Each dataset type comes with two metadata files called `*_Notes_*.txt' and `*_StnDet_*.txt', where the * should be replaced by the data type and a BoM ID number (eg. 99999999299892) respectively. “*_Notes” provides a detailed explanation of the data format for the data type, including a description of the recording instrument, time and reading frequency. File “*_StnDet_*.txt” provides further information about the dataset type including station reference number and name, location (in lat, long); and more importantly, the starting date for the records. In cases in which the station has been closed the final recording date is also presented.

BoM publishes a three-hour interval classification of weather conditions according to the W.M.O. code (BoM, 1982). The present weather is described by 100 symbols abridged from the W.M.O. code indicating the type of weather conditions during the past hour. These symbols are numbered from 0 to 99. From this classification, 12 weather classes that can be considered as thunderstorms were identified. They are classes 17, 27, 29 and classes 91 to 99 as presented in Table 1 Classes 9, 33, 34 and 35 refer to short-period dust storms or sand storms but they have also been included because they impede visibility and hence are related to nearby mesoscale phenomena because of the sudden change in wind conditions (Sanabria & Cechet, 2007a).

Ten symbols for the past weather are also given to represent the most significant weather conditions within the past three hours of observation but not during the most recent hour. BoM numbers these symbols from 0 to 9 (see Table 2).

3.4. GUST WIND SPEED DATASET CLEANING

As mentioned before, results from the statistical model are very sensitive to data quality. In particular, gust speed observations used in these studies are unreliable as instruments are calibrated for mean wind speeds; the procedure does not determine their transient response. This is a serious

Figure 5c shows the half hour gust speed scatter plot, whilst Figure 5d shows the daily mean wind speed calculated from the half-hourly mean wind speed dataset. Figure 5e shows the relationship

Notice that the regression line for the later part of the records is in between the lines of the earlier parts indicating less extreme values; this is because the records of the later part are more reliable since automatic instrumentation and recording systems (replacing chart recordings) was installed in most BoM stations in the 1980's.

Figure 5e: Sydney airport; half-hour gust to mean wind speed ratio.
All wind speeds are in m/s.

In order to obtain an estimate of the dataset quality limitations, Geoscience Australia has developed a Monte Carlo (MC) method which can generate large amounts of synthetic gust data by sampling from appropriate probabilistic functions of mean wind speed and gust to mean wind speed ratio. This synthetic data has been generated by sampling from mean wind speeds and gust factors from recent era of records (i.e. since the late 1980's). The MC technique is able to produce synthetic datasets of this period that compare well with the gust wind speed observations. The MC technique also allows the production of longer records, equivalent to thousands of years of observation, and can be used to calculate improved confidence intervals for high return period hazard. For a full description of the MC method see Sanabria & Cechet (2010).

Table 5. 500 year return period (RP) of combined gust wind with 95% CI considering the complete observed data record.

4.1.1 CONSIDERING ONLY THE OBSERVING RECORD POST- 1980

In order to address concerns over the reliability of data recorded by older, possible poorly calibrated equipment, we recalculated Table 5 using only the part of the dataset after 1980. The selection of 1980 as the cut-off point was made on a basis that it was the start of the decade about which station equipment began being migrated from Dines to cup style anemometry and onsite data recording practices were improved. It was not possible to separate according to the actual equipment used at the site due to the unavailability (at the time) of the station metadata records.

Table 6 presents the exceedance levels of the total or combined maximum daily gust speed of the 500 year RP with 95% confidence interval, data in the range 1980-2006 was used.

When comparing the exceedance levels of the 500 year RP of the gust speeds produced by the full and post 1980 station dataset, it is clear that the exceedance levels do not differ in any consistent manner across multiple stations. Most values are higher for the full dataset case although a few stations present lower values for the full dataset, see for instance station 8 'Coffs Harbour'. This is due to most of the high wind speeds for this station occuring after 1980. The presence of higher values in a smaller dataset results in higher exceedance levels for the RP.

Table 7. 500 year RP of combined wind with 95% CI (observations from 1991-2006)

Figure 8. Distribution of the 500 year RPs presented in Table 9.

Table 10. 500 year RP of combined maximum daily gust wind speed and 3PM mean wind speed with 95% confidence limits (95CI) from the observing record segmented into Dines and Replacement cup anemometer measurement periods (last two columns of the table). All wind speeds in metres per second (m/s).

4.3 COINCIDENT DINES AND CUP-ANEMOMETER OBSERVATIONS

Coincident gust wind speed measurements at 7 northern Australian observing stations were analysed to determine the magnitude of the direct bias. Only Dines "high-speed range" anemometers (0-200 knots) were considered for observing stations where extreme wind gusts are dominated by thunderstorm and tropical cyclone events. The stations examined were Cairns, Townsville, Brisbane, Darwin, Gove, Broome and Learmonth. Cup anemometer data was available in digital form (for each 30 minute interval) whereas the 30 minute maximum gust wind speed for the Dines anemometer record was scaled directly (manually) off the chart record by selecting the maximum peak. Data for 30 minute time segments where the cup anemometer reading was greater than or equal to 15 m/s were analysed. A threshold of 15 m/s was selected so that only thunderstorm and tropical cyclone events were considered (i.e. no synoptic wind events were considered; gusts were independent events). Coincident probability distributions (PDF's) of the gust wind speed ((Dines & cup anemometer; 15 m/s threshold) for the seven sites considered display some interesting characteristics (see Appendix I-C, Figure C1 & Discussion for further information).

Time-series plots of the bias between the Dines and cup anemometer measurements show no time dependent relationships. The bias is uni-directional for some extreme cases where the cup anemometer records the event that the Dines either captures to a much lesser extent or misses altogether. The size of thunderstorm gust fronts can cause significant differences in wind speed over 10's of metres. The uni-directional nature of the extreme bias is due to events captured by the Dines but not the cup anemometer not being considered by the analysis techniques (which was driven by the digital record). Where the analysts found cases where the Dines recorded gusts above 15 m/s but the cup anemometer was below this threshold, the data was included (but this did not occur rigorously; i.e. every 30 minute period for every day was considered on the electronic record and only at or above the cup anemometer 15 m/s threshold for the Dines charts).

The data on the extreme gust wind speeds for the 7 sites were combined into one dataset and extreme value statistical theory (Generalised Pareto Distributions; GPD's) were used to investigate the return period exceedence levels for the combined dataset. Figure 10 shows the return period plots of coincident maximum gust wind speed (above a threshold of 15 m/s for 30 minute time sections) for the combined 7 northern Australian observing stations obtained over a total measurement period of 89 years. In addition, 95% confidence limits (95CI) for the GPD fit to the Dines extreme gust wind observations are also shown. Table 11 details the percentage bias between the cup anemometer and Dines return period estimates (including the 95% confidence limits regarding the fitting of the extreme value distribution to the Dines gust observations).

The observed data allows us to consider gust wind speeds between 45 and 70 m/s. When considering gust wind speeds, the Dines anemometer has a tendency to read about 10 to 15% higher than the cup anemometer (considering coincident data at 30 minute intervals). These systematic differences confirm concerns about the consistency of the peak gust wind speed observational database which underpins the Australian wind loading standard (AS/NZS 1170.2, 2002).

Figure 10. Return period plots of coincident maximum gust wind speed (above a threshold of 15 m/s for 30 minute time sections) for the combined 7 northern Australian observing stations over a total coincident measurement period of 89 years. 95% confidence limits for the GPD fit to the Dines anemometer observations are also provided.

Table 11. Percentage difference (return period gust wind speed9rencholtotal

5. Discussion

Statistical analysis of the daily maximum gust wind speed observations was conducted by employing extreme value distribution (EVD) statistical theory. Generalised Pareto Distributions (GPD's) were fitted to:

(1) Separate time-series of Dines & cup anemometer observations (no overlap for each station)
(2) Coincident Dines & cup anemometer observations

Separate time-series of Dines & cup anemometer observations (no overlap)
We have evaluated both the daily maximum gust and 3PM mean wind speed 500-year return period (500RP) exceedance levels for the total (*combined*) wind speeds for the 31 wind observing stations selected (within AS/NZS 1170.2 Region A). Observations have been segmented into the Dines and replacement cup anemometer observing periods. The 95% confidence interval (95CI) has been determined for both gust and 3PM mean wind speeds for the Dines anemometer segment of the record. For the replacement anemometer 500RP exceedance level gust wind speed estimates, there are 17 observing stations where the replacement anemometer estimates fall below the lower 95% confidence interval (95CI) for the Dines segment of the observing record. For 24 of the 31 observing stations the replacement anemometer estimate fall below the corresponding Dines segment estimate. Considering the 3PM mean wind speeds, there are 18 observing stations where the replacement anemometer estimate falls below the lower 95CI for the Dines segment of the observing record.

The statistical analysis utilising extreme value distributions (GPD's) resulted in more than half of the observing stations considered (later part of the time-series record) having both 500-year RP gust wind speed (17 of 31) and 3PM mean wind speed (18 of 31) exceedance level estimates being in the lower tail of the distribution for the early part of the observing record (period prior to equipment upgrade from Dines to cup anemometer). We should be cautious in interpreting the differences in the return period hazard for the two segments of the record. It is possible that the frequency of extreme wind speeds has actually declined (Smits *et al*. 2005). The most recent part of the record has been dominated by a number of large El Nino events and only one La Nina event, where thunderstorms are known to be more prevalent (Kuleshov *et al*. 2002). The importance of the non-stationary climate needs to be considered when conducting a time series analysis. Circulation changes as discussed in (Plummer *et al.* 1999; Alexander *et al.* 2010), possibly driven by anthropogenic climate change, could also affect the frequency and amplitude of extreme winds. The replacement anemometer part of the record is generally much shorter (10-25 years) than the Dines segment and it is possible that the very high maximum wind speeds have just not yet been sampled, although the

6. Conclusions

This study has examined the observed record of peak gust wind speed in order to establish the existence of a bias between the early part of the record (measurements obtained using pressure-tube Dines anemometers) and the later part of the record (measurements obtained using 3-cup anemometers). The 38 recording stations considered were all situated at airports and were in the most part staffed by Bureau of Meteorology officers. To isolate the issue of anemometer replacement, only observing stations located at airports (consistent exposure) and with more than 30 years of record were considered.

Statistical analysis of the daily maximum gust wind speed observations was conducted by employing extreme value distribution (EVD) statistical theory to examine the difference between two datasets:

(1) time-series of Dines & cup anemometer observations (no overlap for each station);
(2) coincident Dines & cup anemometer observations.

Analysis of time-series of Dines & cup anemometer observations (no overlap)

The statistical analysis resulted in more than half of the observing stations considered (later part of the time-series record) having both 500RP gust wind speed (17 of 31) and 3PM mean wind speed (18 of 31) exceedance level estimates being in the lower tail of the distribution for the early part of

7. Future Directions and Recommendations

It has been identified that the observational record attributable to the Dines anemometer provides a more extreme wind climatology than the part of the record attributable to the 3-cup anemometer. In addition, the Dines anemometer has an effective gust duration approaching 1 second, which is considered suitable for informing design wind speeds. The synchrotac anemometer has a 3-second moving average (1-second sampling) applied to the digital output for maximum wind gust measurements. This is considered the major reason as to why the cup anemometer consistently reads lower than the Dines with respect to the recording of severe wind events.

The results of the *Australian Extreme Wind Speed Baseline Climate Investigation* study indicate that there is a need to firstly review the use of the 3-second moving average for gust wind speed observations to determine the extent that this issue affects the consistency of the observing record (and will continue to do so). It does appear that the WMO standard gust is a retrograde step with regards to informing wind loading. The adoption of the WMO standard gust in the mid-1990's appears to have gone unnoticed by the wind engineering community, or possibly its impact was not fully considered at the time of implementation. The "up-side" of the WMO standard gust is that currently we do have a consistent, standardized gust definition that is being applied worldwide, and this should also eliminate variability due to instrumentation response characteristics.

In moving forward, we need to deal with the issue of improving the consistency of measurements within the gust wind speed observing record. In one very real sense this study has provided the engineering community with the outputs (knowledge and tools) to improve our understanding of the baseline extreme wind climatology within Australia. It has also developed preliminary corrections based on this information which could be utilised to develop a reanalysed observing record which

Acknowledgements:

The *Australian Extreme Windspeed Baseline Investigation Project* is a collaboration between James Cook University, the Bureau of Meteorology, JDH Consulting and Geoscience Australia. A significant portion of the funding (about 60%) was obtained from the Federal Department of Climate Change and Energy Efficiency (DCCEE). The study was conducted in support of DCCEE's climate change professional development program, in the area of building standards. The team at Geoscience Australia would like to thank Rachael Dempsey, Antonio Mozqueira and Anthony Swirepik from the Department of Climate Change and Energy Efficiency for their assistance and guidance with the study.

References:

Alexander L.V., Uotila P., Nicholls N. and Lynch A. 2010. A New Daily Pressure Dataset for Australia and Its Application to the Assessment of Changes in Synoptic Patterns during the Last Century, *Journal of Climate 23:5* 1111-1126

——, 2010. Severe Wind Hazard Assessment using Monte Carlo Simulation. *Environmental Modeling and Assessment*, **15,**

Appendix I - A.

Scatterplots of the gust wind speed datasets

Figure A presents the scatterplot of the maximum daily gust wind speed datasets used in this study. Only wind speeds greater or equal to 25 m/s, the speeds relevant for wind hazard studies, have been plotted. The vertical (dotted) lines are the dates in which the wind recording instruments were either changed, modified or moved to a new position (see anemometer metadata; Section 3.2).

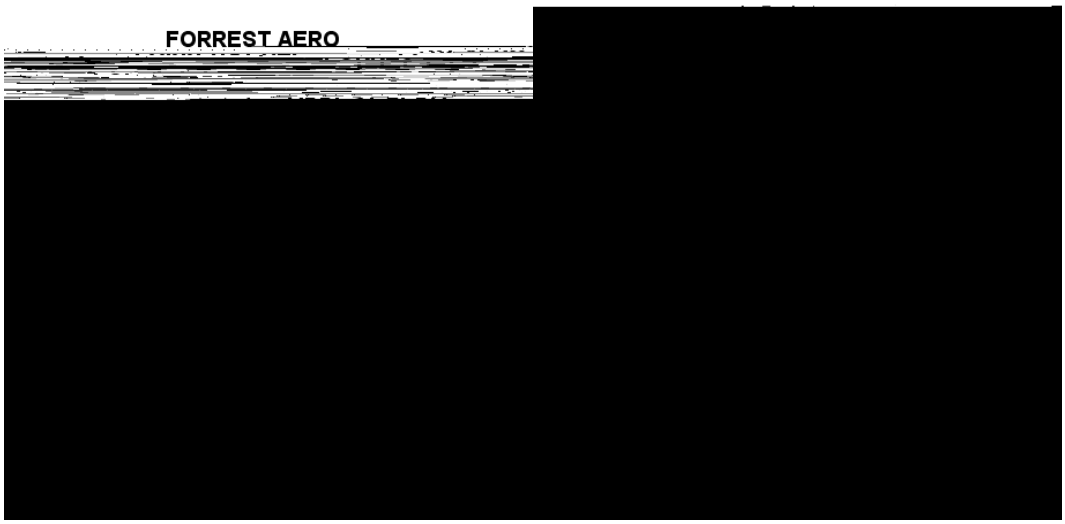

Figure A. Scatterplots of the maximum daily gust wind speeds

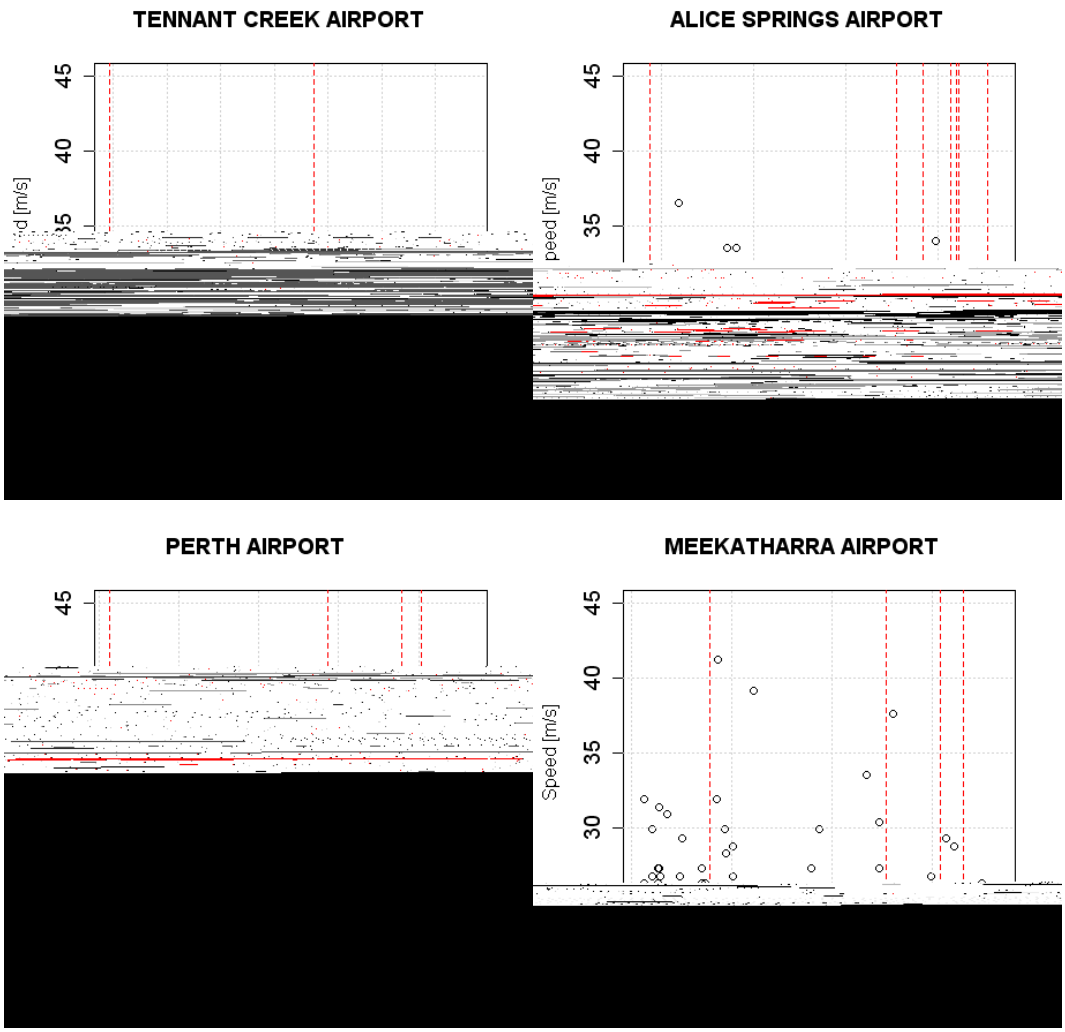

Figure A (Cont.). Scatterplots of maximum daily gust wind speeds

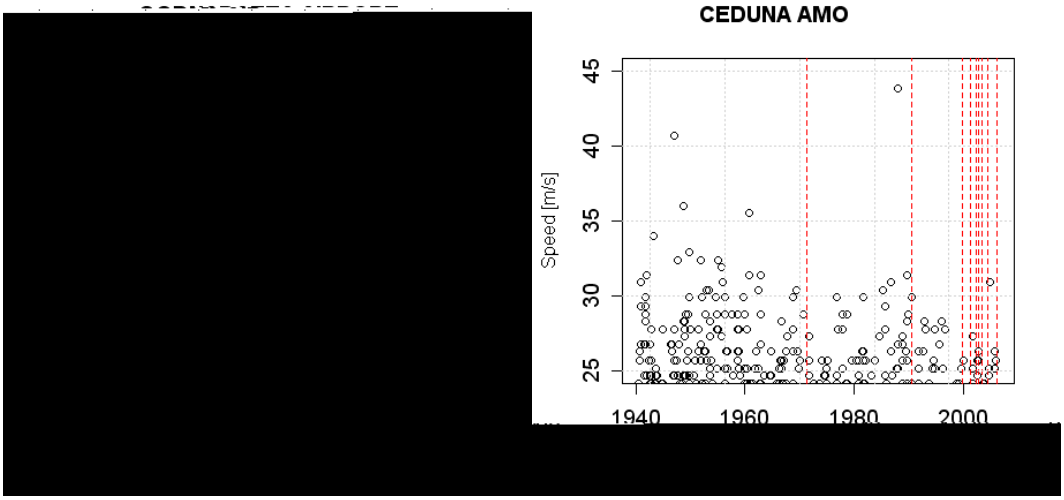

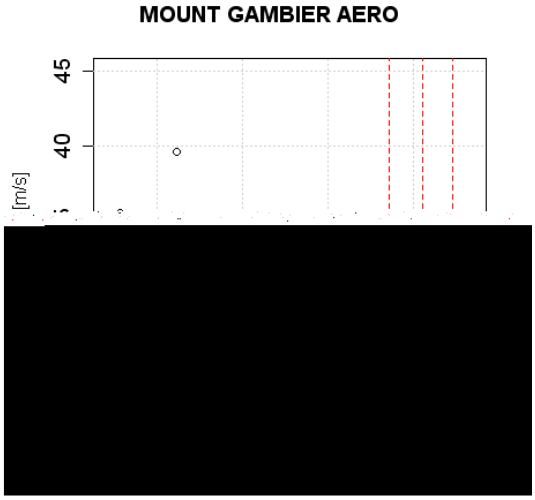

Figure A (Cont.). Scatterplots of maximum daily gust wind speeds

Figure A (Cont.). Scatterplots of maximum daily gust wind speeds

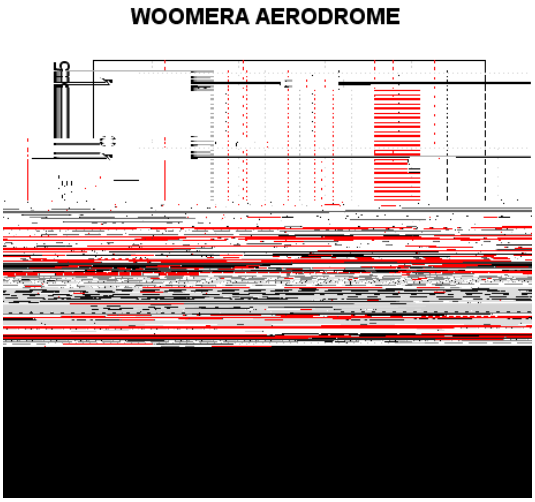

Figure A (Cont.). Scatterplots of maximum daily gust wind speeds

Appendix I - B.

Return period (RP) plots of maximum daily gust wind speed for the 31 "Region A" observing stations considered in Sections 4.1 & 4.2 (see Figure 5 for observing station locations depicted on a map of Australia).

Figure B1. RP curves of the three types of winds; synoptic, thunderstorm and combined for Perth, Sydney, East Sale and Ceduna airports.

Figure B2. RP curves of synoptic, thunderstorm and combined winds for Williamtown, Nowra, Mount Gambier and Laverton airports.

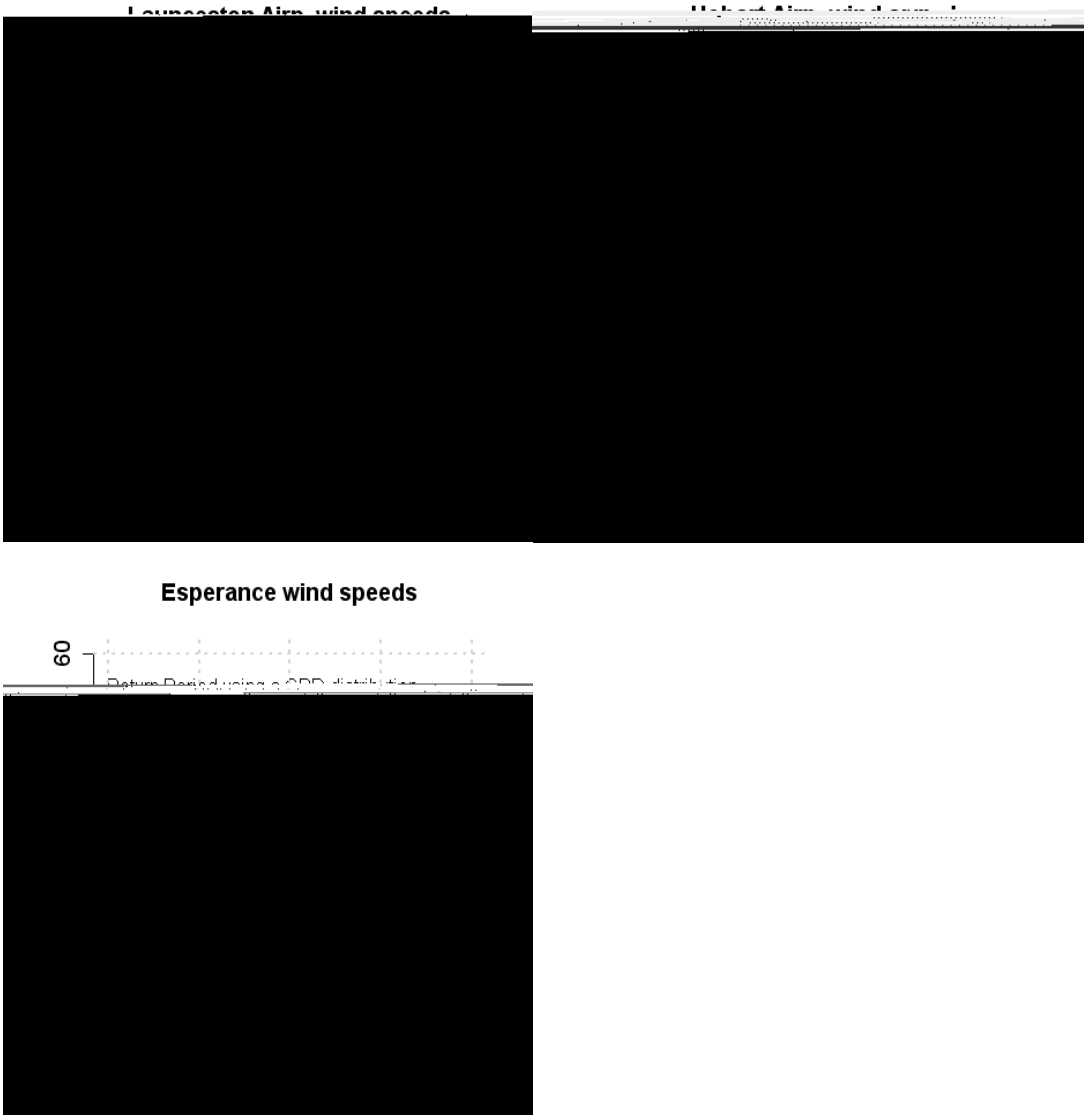

Figure B3. RP curves of synoptic, thunderstorm and combined winds for Launceston, Hobart, Esperance and Coffs Harbour airports.

Figure B4. RP curves of synoptic, thunderstorm and combined winds for Canberra, Forrest, Oodnadatta and Albany airports

Figure B5. RP curves of synoptic, thunderstorm and combined winds for Tennant Creek, Kalgoorlie-Boulder, Charleville and Adelaide airports.

Figure B6. RP curves of synoptic, thunderstorm and combined winds for Alice Springs, Giles, Cobar and Moree airports.

Figure B7. RP curves of synoptic, thunderstorm and combined winds for Halls Creek, Meekatharra, Mildura and Longreach airports.

Figure B8. RP curves of synoptic, thunderstorm and combined winds for Mount Isa, Wagga Wagga and Woomera airports.

Figure C1 (cont). Probability distributions of the gust wind speeds for the coincident anemometer datasets

(ii) Bias between coincident Dines and cup anemometer observations

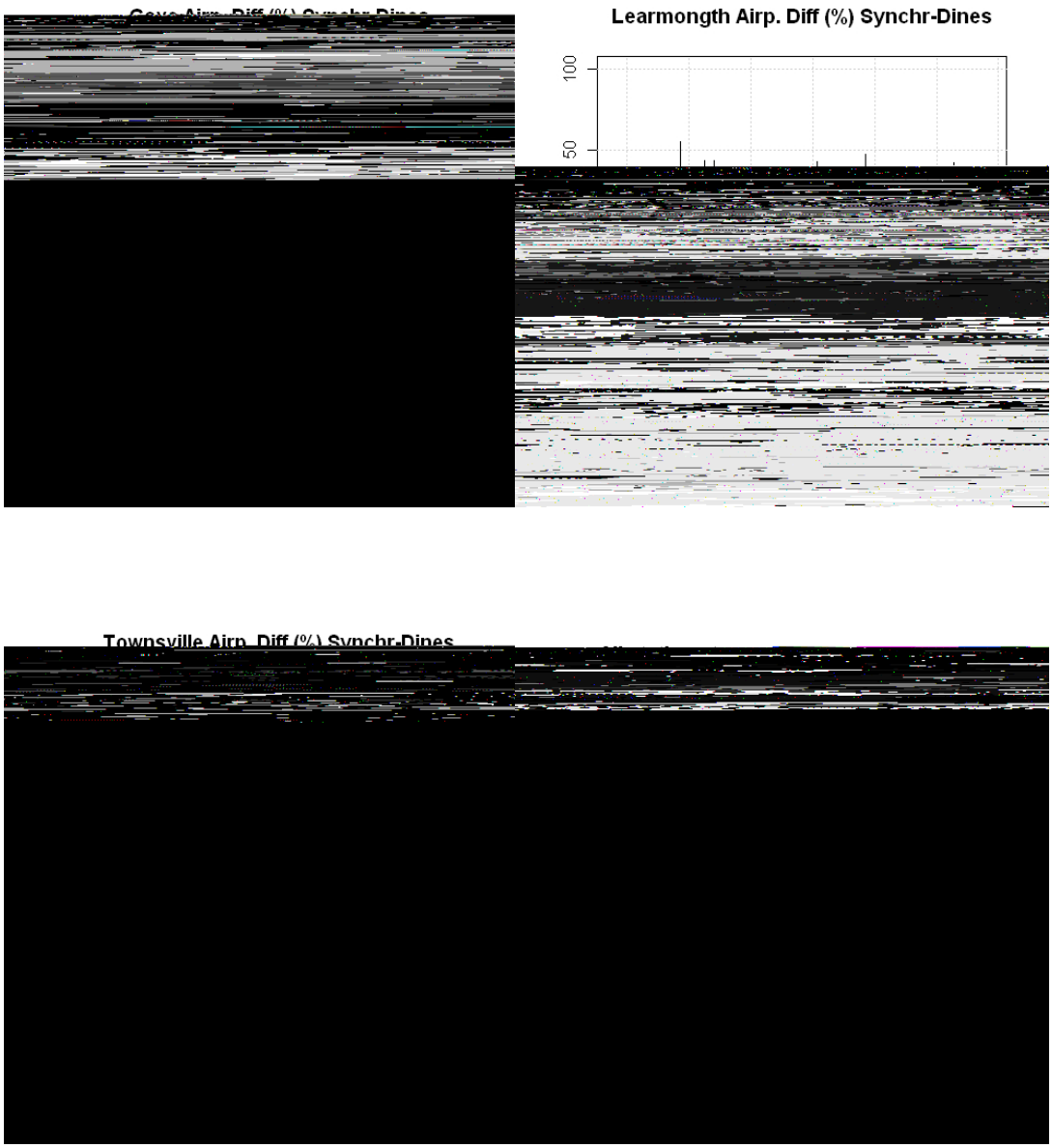

Figure C2 (Cont.). Time-series plot of bias between Dines and cup anemometer coincident measurements

Appendix II-1

Literature review of Dines anemometer response, and related studies

John Holmes
P.O. Box 269, Mentone
Victoria 3194
www.jdhconsult.com

As stated by Miller (2008), who managed to locate some of the early NPL reports in the U.K. National Archives, early work at NPL suggested that the Dines pressure-tube anemometer (PTA) became more responsive at higher frequencies as the wind speed increased. A later report was found by Miller to contain results from tests in one of the N.P.L. wind tunnels in which oscillating wind speeds with periods of 10, 4 and 2 seconds were achieved. A complete Dines PTA head, 15 metres of pipe, and a float system were installed. It was reported that there was some dependency of the frequency response on the mean wind speed, but not so large as found in earlier work with 30-metre long connecting pipes.

, I D µ SKRZH U ¶ G H I L Q L W L R Q R I H I I H F W L Y H J X V W M H X U D W L R Q (Beex, 2007) then the N.P.L. studies indicated the effective gust time varied from about 5 to 1.5 seconds as the wind speed increased from 10 to 37 m/s. There was apparently little effect of the length of the connecting tubing, with internal diameter of 25 mm.

Ikeda, 1937, and Sanuki, 1952

The only serious previous attempts to mathematically model the response of the Dines anemometer, including the connecting tubing, appear to have been made by Ikeda (1937) and Sanuki (1952) in Japan. The earlier reference appears to be available in Japanese only, but an English language version of the Sanuki paper is available.

The work by Iberall (1950) was probably the first serious attempt to develop a comprehensive theory of pressure transmission down long tubes of small diameter. Iberall first gives an µHOHPHQWDU\¶ VROXWLRQ IRU D VLQJOH WXEH RI XQLIRUP GL The flow in the tube transmitting the pressure fluctuations is assumed to be laminar and

the tubing, which the present project has found is only a problem if very long, or very narrow, tubes are used. The most useful paper reviewed is that of Borges (1968), who focused on the response characteristics of the float movement, and identified the two natural frequencies associated with in-phase and out-of-phase motion of the float and the water; these aspects have been further studied experimentally and theoretically in the present project.

There has apparently been little interest in the U.K. in studying the comparative readings of gust wind speeds recorded by the Dines and cup anemometers, probably because of the earlier replacement of the Dines type by cup anemometers, dating back to the 1950s. Also the wind loading standard there converted from a peak gust to an hourly-mean basic wind speed, some years ago. However, the paper from Ireland by Logue (1986), in which statistical comparisons of gusts recorded over a year were compared, and higher readings of peak gusts by the Dines anemometer on average, is particularly useful for the present project.

There is an extensive literature on the response to pressure measurement systems with long connecting tubing of small diameters to fluctuating (sinusoidal pressures). The theory developed by Bergh and Tijdeman (1965) based on laminar flow, is the most comprehensive. It has been validated for measurement systems with small diameter (i.e. 1-6 mm) tubes in laboratory conditions. In this project (see Appendix II-2), this theory was applied, and validated, for tubing lengths and diameters (12-30 mm) used for the connecting tubing in Dines anemometer systems.

The use of a digital 3-second moving average filter as proposed by Beljaars (1987) is significant for this project, as such a filter has been applied in Australia to cup anemometers, and significantly reduces the maximum gusts reported, compared with those reported before 1990 from Dines anemometers.

References

where V_t is the terminating volume

V_t is the volume of the connecting tubing

L is the length of the tubing

k is a polytropic constant for the volume

Q LV D FRPSOH[µSRO\WURSLF IDFWRU¶ IRU WKH WXELQJ

between 1.0 and 1.4

ϕ LV D FRPSOH[µZDYH QXPEHU¶ GHSHQGLQJ RQ WKH WXE

Figure 2-2 shows the effect of the internal diameter of the tubing on the resonant frequency, and the maximum amplitude ratio at that frequency. It can be seen that both increase with increasing tubing diameter.

Figure 2-2. Effect of tubing internal diameter on resonant frequency and maximum amplitude (tube length: 10m; terminating volume: 0.0017 m^3)

It was also of interest to calculate the response of a system with 30m (100 feet) of tubing of 25mm (1-inch) internal diameter, as used in the tests at NPL recorded by Giblett (1932) and reported later by Whittingham (1964). The amplitude response (to sinusoidal excitation) is shown in Figure 2-3, plotted to the same scale as Figure 2-1.

Figure 2-3 indicates resonant peaks of both lower amplitude and frequency than those for 10m long tubing. The lowest resonant frequency of 2.4 Hertz is much closer to those of the float frequencies, with the potential for some interactions. Thus, there may be some effect of a 30 metre length of connecting tubing on the response of the anemometer float system to fluctuating winds and dynamic pressures, even though a 10 metre length (or shorter) has a negligible effect.

Summary

The main conclusion of this part of the project is that the connecting tubing used on Dines anemometers in Australia, consisting of about 10 metres of tubing of 25-30mm internal diameter, has resonant frequencies considerably in excess of those of the float system. Over the range of the float frequencies the amplitude ratio in Figure 2-1 are very close to 1.0, and hence there should be negligible effect of the tubing on the overall system response. This has been confirmed by the direct measurements in this project reported elsewhere (Task 3).

Good agreement between theoretical predictions, based on laminar fluctuating flow, of the frequency response of tubing typical of that used in the Dines system with experiments, leads to the conclusion that the flow in the tubing system is essentially laminar. This contradicts a conclusion of Sanuki (1952), who suggested that the flow would be better modelled as turbulent flow.

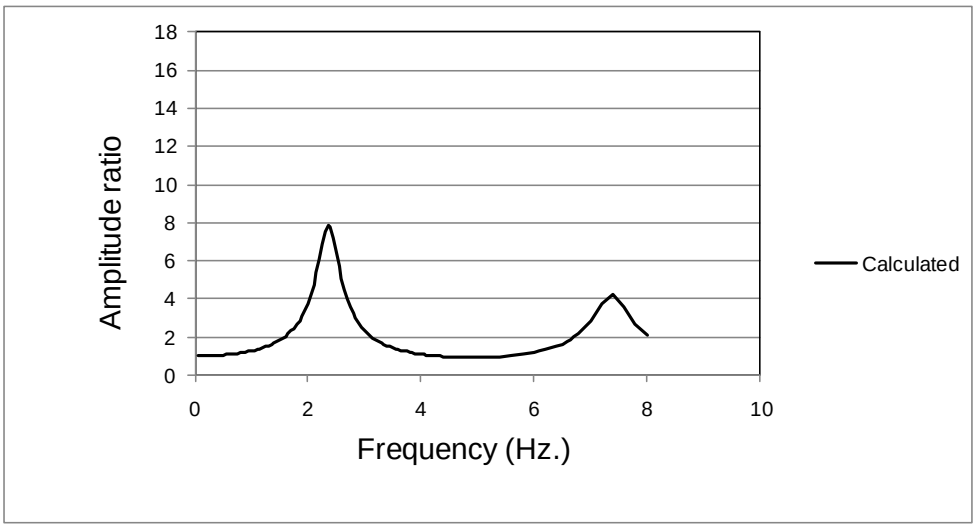

Figure 2-3. Calculated amplitude response for a system with 30m long and 25mm diameter connecting tubing (terminating volume: 0.00177 m^3)

References

H. Bergh and H. Tijdeman, 1965: Theoretical and experimental results for the dynamic response of pressure measuring systems. National Aero- and Astronautical Research Institute, Netherlands, Report NLR-TR F.238.

M.A. Giblett, 1932: The structure of wind over level country. Geophysical Memoirs 63, Meteorological Office U.K.

M. Sanuki, 1952: A new development of the theoretical and experimental lag of Dines pressure tube exposed in fluctuating winds. Papers in Meteorology and Geophysics, 3, 115-124.

H.E. Whittingham 1964: Extreme wind gusts in Australia. Bureau of Meteorology Bulletin No. 46.

Appendix II-3

Statistical comparison of peak velocities recorded by Dines, cup and sonic anemometers using time histories

John Holmes

Results and Discussion

Figure 4 shows parts of the time histories of the Dines anemometer, and of the simulated cup anemometer traces, with some of the peaks selected for comparison. The identified peak velocities and the ratios between the Dines peak and the corresponding ones expected to be recorded by the cup D Q H P R P H W H U V \ V W H P D U H V K R Z Q L Q 7 D E O H $ O V R V K R Z Q D peak gust recorded by the sonic anemometer.

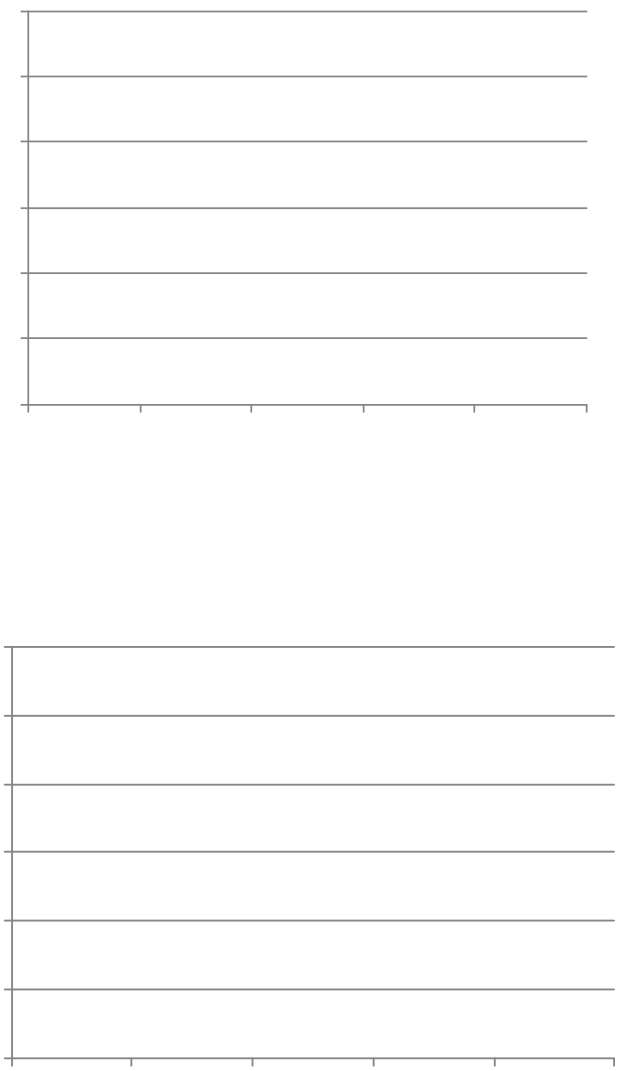

Figure 4. Extracts from wind-speed (ordinates in m/s) versus time (in seconds) histories of the Dines anemometer (blue) and of the cup anemometer (red), showing peaks selected for comparison

Table 1. Comparison of peaks recorded by different anemometer types

Peak No.	Sonic (m/s)	Simulated 3-cup	Dines	Dines/cup	Dines/sonic
1	28.65	25.17	26.32	1.045	0.919
2	26.79	24.61	26.36	1.071	0.984
3	28.45	25.03	26.77	1.070	0.941
4	30.40	27.04	28.79	1.065	0.947
5	32.45	28.70	30.75	1.072	0.948
6	32.05	28.64	30.00	1.047	0.936
7	30.40	26.47	27.57	1.042	0.907
8	28.45	26.29	27.52	1.047	0.967
9	30.58	28.07	29.67	1.057	0.970
10	31.47	28.04	29.41	1.049	0.934
11	31.93	28.79	30.24	1.050	0.947
12	30.70	27.00	28.82	1.067	0.939
13	28.71	26.41	27.31	1.034	0.951
14	28.97	26.05	27.09	1.040	0.935
15	29.97	26.96	28.30	1.049	0.944
16	28.97	26.57	27.90	1.050	0.963
Average	29.93	26.87	28.30	1.053	0.946

Other work for this project shows that the response of the Dines anemometer is dominated by the resonant response frequencies of the float system, particularly the first mode (although any vibrations are heavily damped). Present measurements indicate that the first-mode frequency of the low-speed type is about 0.5 Hertz, about half that measured at N.P.L. in the 1930s, and reported by Whittingham (1964).

Finally, a comment can E H P D G H D E R X W W K H µ H I I H F W L Y H J X V W G X U D D Q H P R P H W H U 8 V L (1964): defining W based on the reciprocal of the half-power frequency (also advocated recently by Miller (2007)), µ H I I H F W L Y H J X V W G X U D W L R Q ¶ 7 the time constant, or effective moving averaging time, τ, by the following (for a first-order measurement system):

$$T \cong 2\pi \tau = 2\pi (\delta/U) \qquad (1)$$

where δ is the distance constant of the anemometer.

It should be noted, however, that the World Meteorological Organization (Beljaars, 1987a) following Beljaars 1987b), has defined µ a J X V W G X U D W L R Q ¶ equivalent to the moving average time τ. Thus % H O M DøB„ 5Y™v" U™—b!€%VY™v! 0 jhastef]TJ 0 -15(i)-,

Figure 5. Simulated time histories of the cup anemometer output with no filtering (red), and with 3-second moving average filtering applied (black)

Appendix II-4

Gust factors for Dines and cup anemometers using the spectral approach

John Holmes
P.O. Box 269, Mentone
Victoria 3194
www.jdhconsult.com

Introduction

pressure of 1.0 kiloPascals, equivalent to a mean wind speed of 33 m/s. Although these were obtained experimentally for the defined mean pressure and equivalent wind speeds, they have been assumed to be applicable for all mean wind speeds for the purposes of the calculation of gust factors and gust ratios shown following. However, iterative calculations, in which frequency shifting of the transfer function was assumed (in proportion to the square root of the mean wind speed), indicated very little change in the computed gust ratios.

Comparison of gust factors and gust ratios

Using the above methodology, the expected gust

on average than those from the cup anemometer. The distance constant for the U.K. Mark 2 cup anemometer is 12 metres (Sparks, 1996, 1997, communicated by C.A. Miller). As an indicator of the turbulence intensities at the site, Figure 1 in the Logue paper indicates a mean gust factor as recorded by the Dines anemometer, of about 1.7.

The following table shows the computed gust ratio, using the random process approach, for the conditions in the Logue study. The other parameters were taken the same as in the previous example.

Table II.

Mean wind speed Turbi021 c0003>rnTT1 1 Tf1 TTable IIcatTd <t14-1nel25 Td .e.

Table III. Overshoot ratios for Low-speed Dines versus Synchrotac 706 with 3-sec averaging

Mean wind speed	Turbulence intensity	Avg. Gust factor (ls. Dines)	Avg. Gust factor (cup with 3s filter)	Max. gust (cup) (m/s)	Overshoot ratio	Overshoot Ratio (no 3s filter on cup)
20	0.10	1.3234	1.240	24.8	1.068	1.034
25	0.10	1.3238	1.237	30.9	1.070	1.030
30	0.10	1.3241	1.234	37.0	1.073	1.026
35	0.10	1.3242	1.231	43.1	1.076	1.023
20	0.15	1.4851	1.359	27.2	1.092	1.046
25	0.15	1.4857	1.356	33.9	1.096	1.040
30	0.15	1.4861	1.352	40.5	1.100	1.035
35	0.15	1.4863	1.347	47.1	1.104	1.031
20	0.20	1.6467	1.479	29.6	1.113	1.056
25	0.20	1.6477	1.475	36.9	1.117	1.049
30	0.20	1.6482	1.469	44.1	1.122	1.043
35	0.20	1.6484	1.462	51.2	1.127	1.038

Table IV. Overshoot ratios for High-speed Dines versus Synchrotac 706 with 3-sec averaging

Mean wind speed	Turbulence intensity	Avg.

Conclusions

The random process approach to gust factors and Dines/cup gust ratios gives good agreement with independently obtained values of gust ratios, and easily enables adjustment for varying parameters, such as mean wind speed, turbulence intensity, turbulence length scale, and the distance constant of the cup anemometer.

The approach has been applied to comparisons of the average gust factors and gust ratios recorded by the Dines and those expected from the type of cup anemometer currently used by the Bureau of Meteorology in their Automatic Weather Systems, with the 3-second moving average filter applied. As a result of the analysis, significant 'overshoot' in measured gust wind speeds are expected to occur – up to 13% for the low-speed Dines, and up to 21% for the high-speed Dines. These are compatible with statistical analyses by Geoscience Australia, and with anecdotal evidence from individual stations in the cyclone regions, where the instruments have operated in parallel.

References

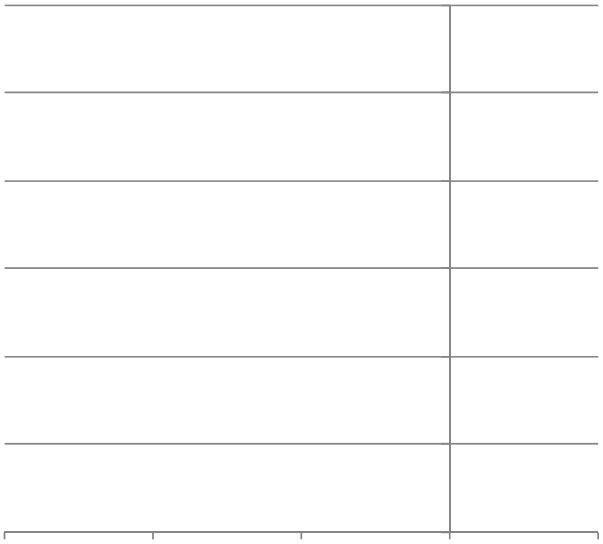

Figure 3. Spectral density as modified by the cup anemometer – mean wind speed of 25 m/s

Figure 4. Spectral density as modified by the low-speed Dines anemometer – mean wind speed of 25 m/s

Appendix II-5: Modelling the Transient Response of the Dines Anemometer

Jeffrey D. Kepert
Centre for Australian Weather and Climate Research,
Bureau of Meteorology,
700 Collins St,
Melbourne Vic 3000.
Email: J.Kepert@bom.gov.au

April 28, 2011

1. Introduction

This report details the development of a physical model of the Dines anemometer oat

where R_d is the gas constant for dry air and T_d is the air temperature. We will use $s(t)$ as the principal forcing of the system.

The forces on the oat are its weight gm_1, the upwards pressure of the trapped air $p_a A$, and friction which we model as a linear damping to zero with time scale τ_1, and a linear damping to the liquid motion with time scale τ_3. Newton's second law,

$$$$

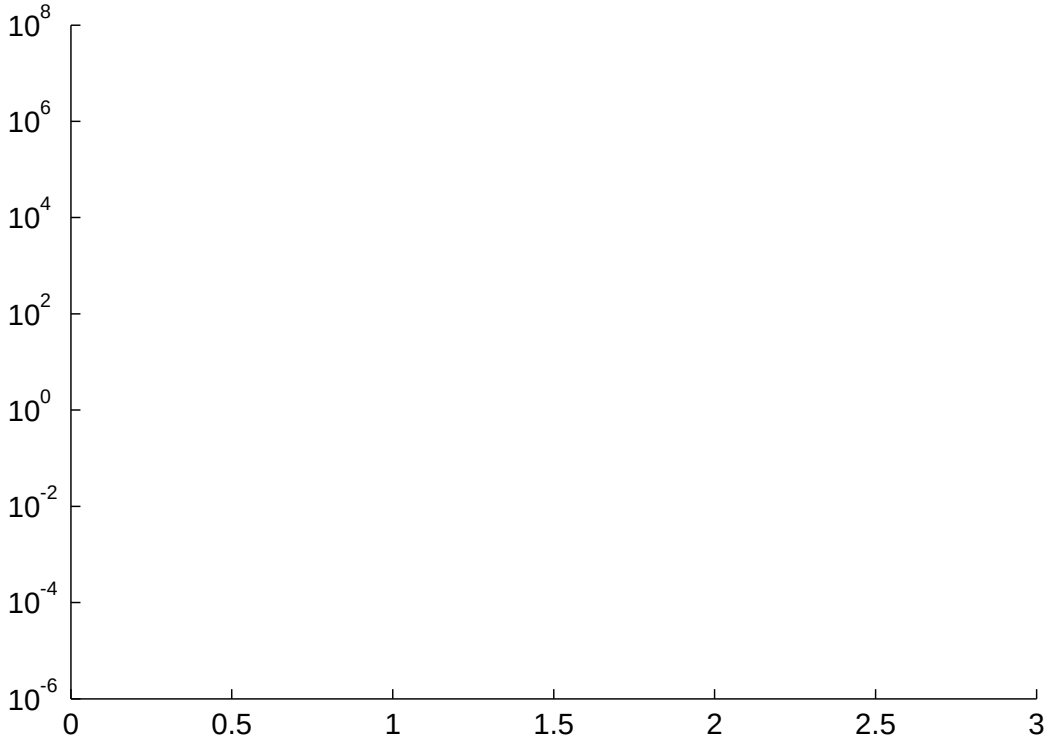
10^{8}
10^{6}
10^{4}
10^{2}
10^{0}
10^{-2}
10^{-4}
10^{-6}
0
0.5
1
1.5
2
2.5
3

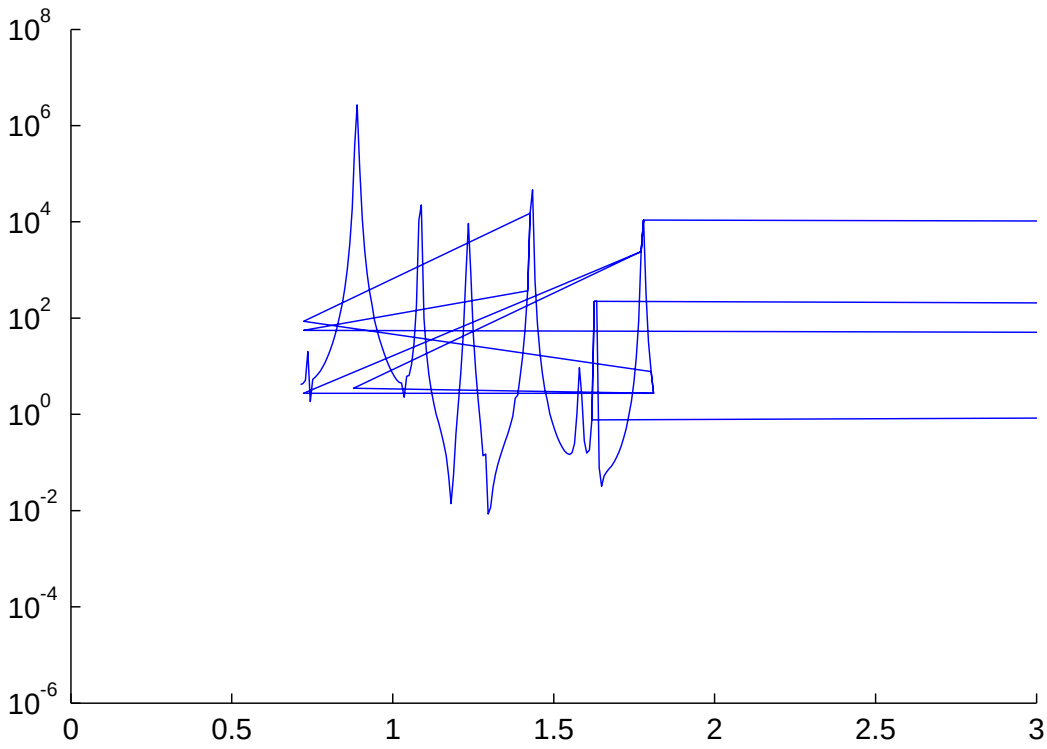
10^{8}
10^{6}
10^{4}
10^{2}
10^{0}
10^{-2}
10^{-4}
10^{-6}
0
0.5
1
1.5
2
2.5
3

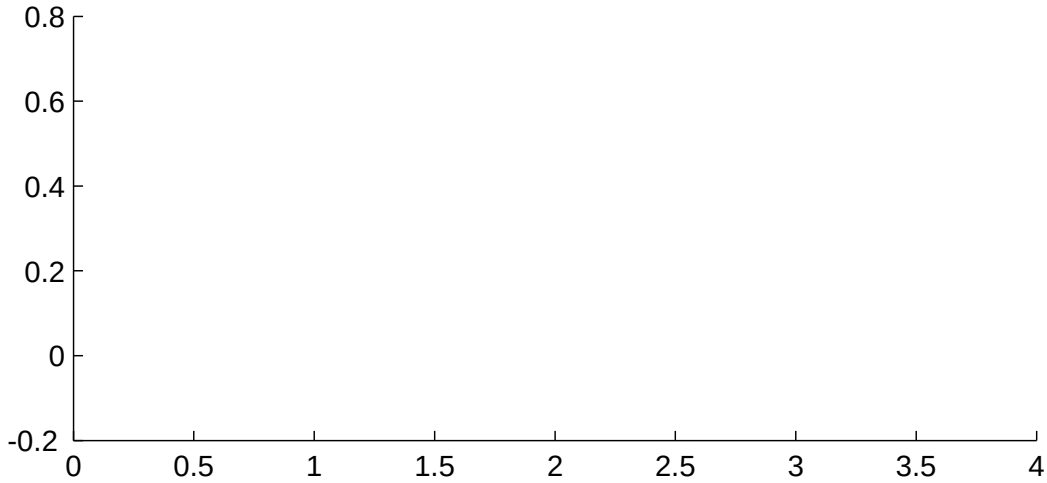
0.8
0.6
0.4
0.2
0
-0.2
0
0.5
1
1.5
2
2.5
3
3.5
4

in Fig 3 are also apparent. Other interesting features include the regular variation in the width of the peak about t_1 and to a lesser extent t_2

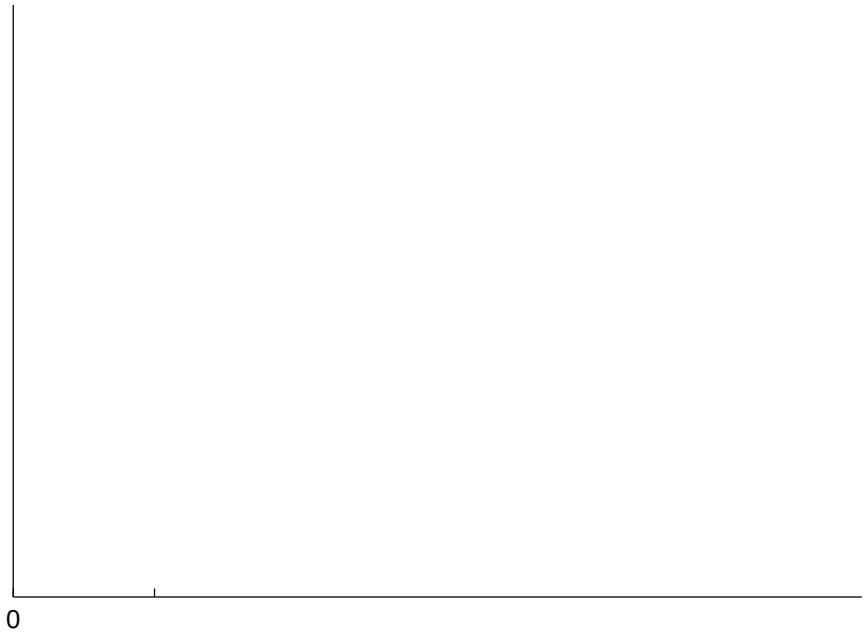
0

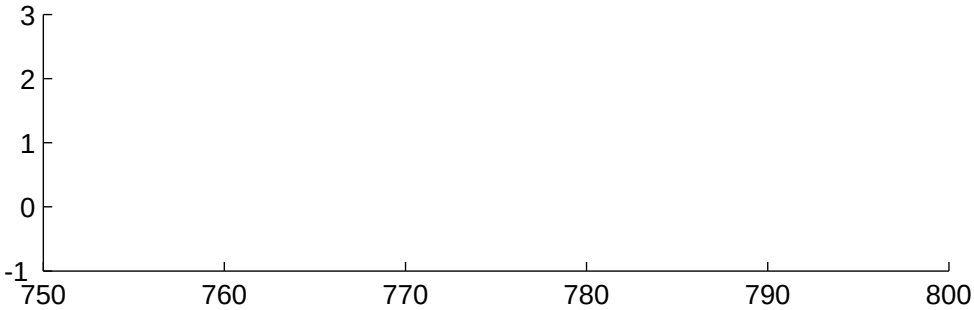
3
2
1
0
-1
750
760
770
780
790
800

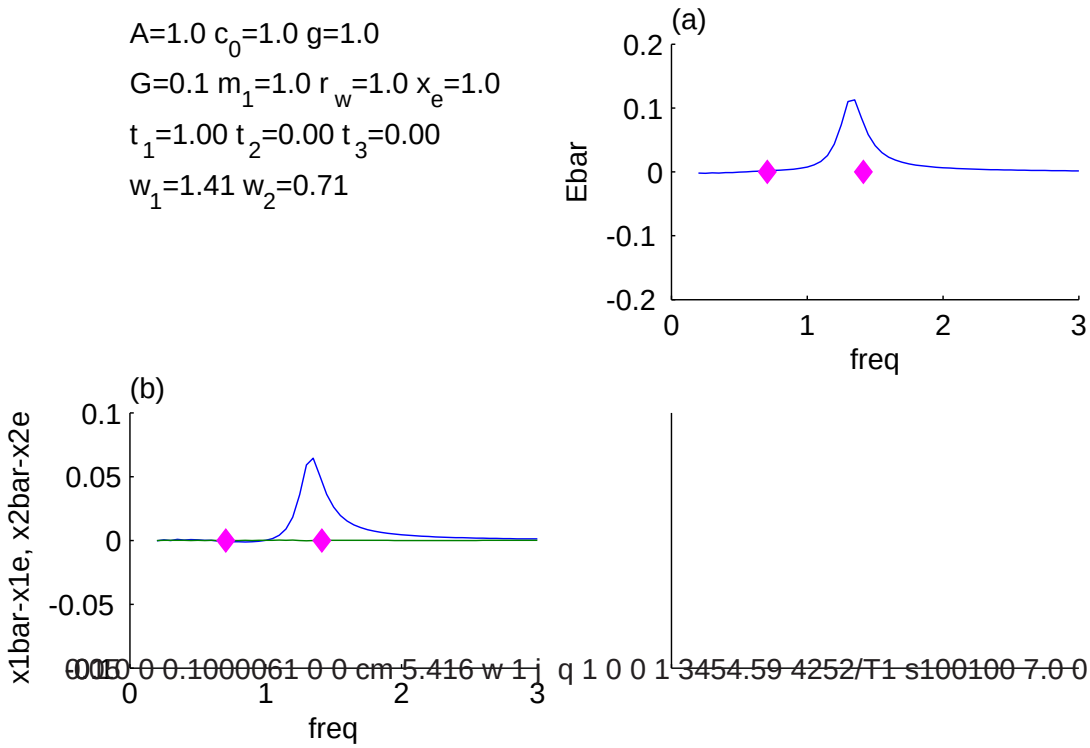

~~0 0 0 0.1000061 0 0 cm 5.416 w 1 j~~ q 1 0 0 1 ~~3454.59 4252/T1 s100100 7.0 0~~ 0 0 BT 9S Q Q B-.0.

A=1.0 c_0=1.0 g=1.0

G=0.5 m_1=1.0 r_w=1.0 x_e=1.0

t_1=1.00 t_2=0.00

w_1=1.41 w_2=0.71

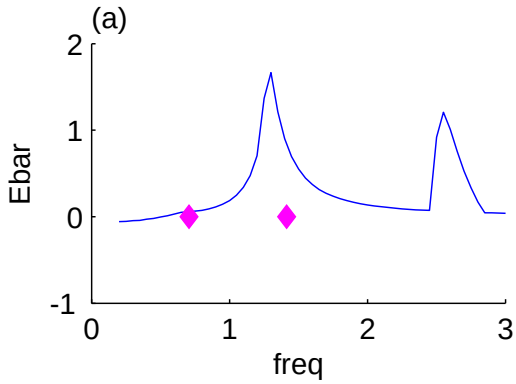

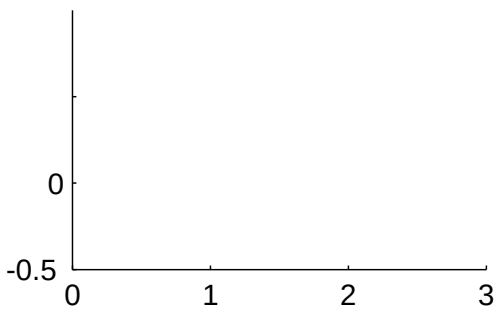

A=1.0 c_0=1.5 g=1.0

G=0.1 m_1=1.0 r_w=1.0 x_e=1.0

t_1=0.30 t_2=0.10 t_3=0.50

w_1=1.26 w_2=0.65

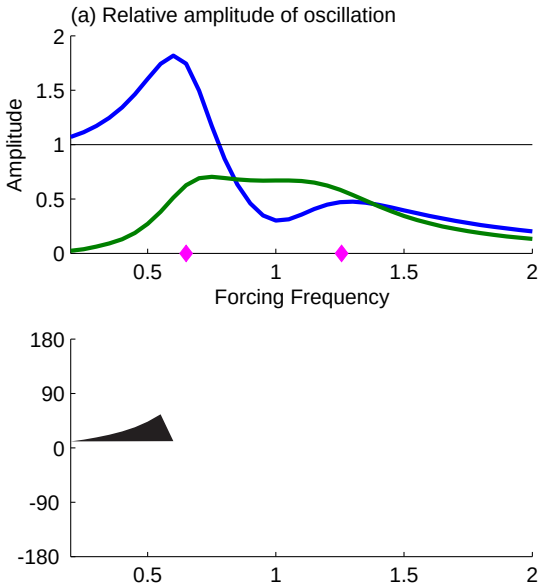

Figure 14: The relative amplitude (top) and phase (bottom) of the oat movement, as a function of forcing frequency, for a Fuess anemometer with various tubing lengths. From Borges (1968).

The phase response shifts from in-phase at low frequencies, out-of-phase at high.

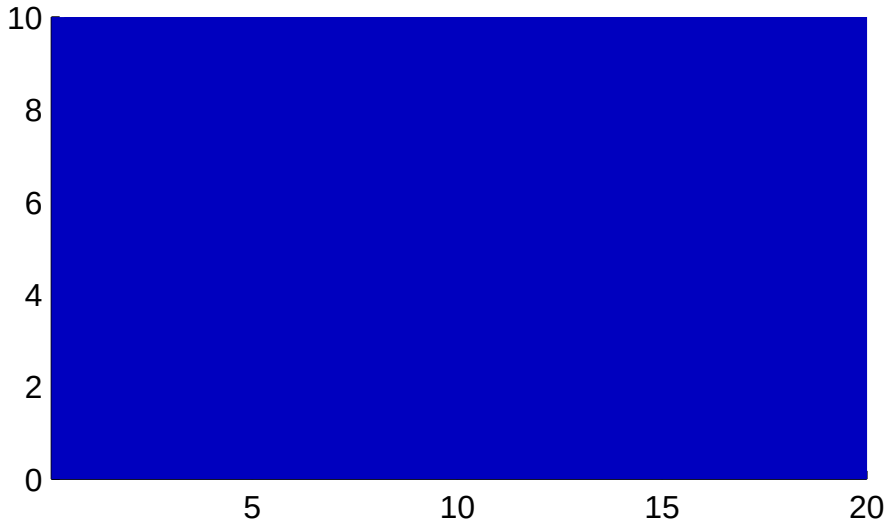
10
8
6
4
2
0
5
10
15
20

$$b_2 = \frac{S \quad \sqrt{S^2 + 8Am_1 x_e(gm_1 + Ap_{env})^4}}{2m_1(gm_1 + Ap_{env})^2} \tag{34}$$

where

$$S = (gm_1 + Ap_{env})^2(m_1 \quad 2Ax_e) + 2Agm_1 c \tag{35}$$

It follows from

$$\begin{aligned}[S + 4Ax_e(gm_1 + Ap_{env})^2]^2 \quad & [S^2 + 8Am_1 x_e(gm_1 + Ap_{env})^4] \\ &= 16A^2cgm_1(gm_1 + Ap_{env})^2 \quad {}^2x_e \\ &> 0\end{aligned} \tag{36}$$

that $!_1^2 > 0$, so $!_1$ is real.

Physically, the effect of including p_{env} is to increase the stiffness of the spring. Previously, if the volume of the trapped air halved, then p doubled. Now p becomes $2(p_{env} + p) \quad p_{env} = p_{env} + 2p$. For $p_{env} \quad p$

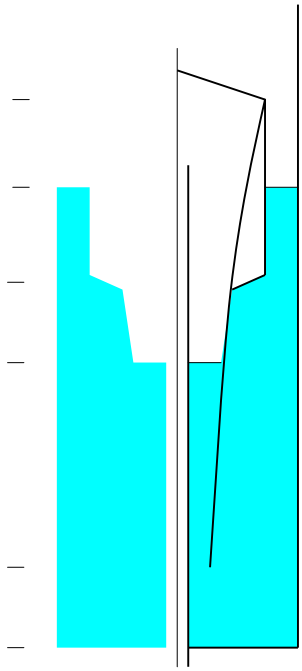

Here, the rst term represents the pressure of water on the bottom of the otation collar $g(x_3 - x_1)$ times the area of that collar $A_x Y(x_3)$, while the second is the pressure of water on the inner surface of the oat $g(x - x_1)$, in an upwards direction, integrated over the length of the oat. Note the y09 Tf 4.16()Tj /T1_4 7.97 Tf 6.24 -1.68 Td (BT 0 0 0 1 k /GS0 gs /T1_0 10.909 Tf 91.8 7

Using (49) to replace x_d in (51) yields

$$x_1(v) = \frac{(C \quad T)^2 + 2CqTx_2(v) + (C \quad T)^{3=2}\sqrt{C \quad T + 4Cqx_2(v)}}{2C^2q} \tag{54}$$

Taking (40), using (41) for V_{sa} and (47) for V gives

$$mg + A[x_3 \quad x_1(v)] = \int_{x_2(v)}^{x_3} Y(x)\,dx \tag{55}$$

or, differentiating with respect to v,

$$Ax_1^0(v) = Y(x_2(v))x_2^0(v): \tag{56}$$

Eliminating x_1^0 and x_d^0 between (48), (53) and (56) gives an expression for $Y(x_2)$ in terms of x_d,

$$Y(x_2) = \frac{A\{C \quad T + 2qT[x_d(v) \quad x_d(0)]\}}{C \quad T + 2qC[x_d(v) \quad x_d(0)]} \tag{57}$$

or, using (49) to replace x_d then (54) to replace x_1, and writing in terms of x not x_2 for convenience,

$$Y(x) = A\frac{C \quad T + T\sqrt{1 + \frac{4Cqx}{C \quad T}}}{C\sqrt{1 + \frac{4Cqx}{C \quad T}}}: \tag{58}$$

This equation, (58), is the required expression for the shape of the oat. When C, it reduces to

$$Y(x_2) \quad \frac{A}{\sqrt{1 + 4qx_2}} \tag{59}$$

3.2 Some properties of Y

Some useful properties of Y follow.

The derivative is

$$Y^0(x) = \quad 2Aq\left(1 + \frac{4Cqx}{C \quad T}\right)^{3=2} \tag{60}$$

The integral is

$$\int_0^x Y = \frac{A}{2C^2q}\left\{(C \quad T)^2\sqrt{1 + 4Cqx=(C \quad T)} \quad 1 \quad + 2CTqx\right\} \tag{61}$$

and the inverse function of $\int_0^x Y$ is

$$y \mapsto \frac{A(C \quad T)^2[1 \quad \sqrt{1 + 4qTy=(A(C \quad T))}] + 2CqTy}{2AqT^2} \tag{62}$$

As the oat has a tube up the middle, similar expressions for Y for T are also needed. The integral is

$$\int_0^x Y \quad T = \frac{A(C \quad T)^2\sqrt{1 + 4Cqx=(C \quad T)} \quad 1 \quad + 2C(A \quad C)Tqx}{2C^2q} \tag{63}$$

that is, the amplitude of the oscillation is small compared to the length of the slug of liquid.

As the condition (76) applies in real Dines manometers, the pressure in the tank could be assumed to be hydrostatic even though the oscillating uid requires nonhydrostatic pressure gradients in the uid. However, a dif culty arises with this approach. If the hydrostatic equation is integrated downwards along each arm of the manometer, two estimates for the pressure at the bottom will be obtained. The difference between these estimates is of the order of the departure from hydrostatistic balance and, while formally negligible, is an uncertainty in the model formulation. To avoid this untidiness, the nonhydrostatic pressure gradient will be assumed to be constant, but of opposite sign inside and outside of the oat.

Then

$$p_{in} = p_d \quad (g + \quad)y \tag{77}$$

$$p_{out} = p_d \quad (g \quad)y \tag{78}$$

where p_{in} and p_{out} are the pressures inside and outside of the oat, p_d is the pressure at the bottom of the tank, and is the nonhydrostatic part of the vertical pressure gradient.

Applying the boundary conditions $p_{in}(y_2) = \quad p$ and $p_{out}(y_1) = 0$ yields

$$p = p_d \quad (g + \quad)y_2 \tag{79}$$

$$0 = p_d \quad (g \quad)y_1 \tag{80}$$

whence

$$p_d = \frac{y_1 \; p + 2 y_1 y_2 \; g}{y_1 + y_2} \tag{81}$$

$$= \frac{p + \quad g\,(y_1 \quad y_2)}{y_1 + y_2} \tag{82}$$

which are suf cient to de ne the internal pressure throughout the water.

3.4 Internal pressures in the liquid. II: What is the effect of constrictions?

The previous section analysed the departures of the pressure from hydrostatic balance due to the oscillation of the uid, assuming a constant tube diameter. However, the ow in and around of the oat in a Dines manometer has accelerations due to the varying width of the passage between the walls of the tank and the oat, and within the oat itself. These variations will also induce pressure perturbations. The magnitude of these perturbations is now estimated and shown to be negligible.

Consider for simplicity steady, inviscid and irrotational ow along a U-tube passageway similar to that sidcussed in section 3.4, but of varying cross-sectional size $S(z)$. Bernoulli's theorem then states that

$$H = \frac{1}{2}q^2 + \frac{p}{} + gjzj \tag{83}$$

is constant along a streamline, where q is the speed of the uid. Making the approximation that the speed is constant across the width of the tank, $S w_k$ is constant along the axis of the tube, so (83) becomes

$$H = \frac{1}{2} \quad \frac{S_0 w_0}{S} \quad ^2 + \frac{p}{} + gjzj \tag{84}$$

Taking the boundary condition p constant at $z = z_t$, which without loss of generality can be taken as $p(z_t) = 0$, the pressure within the uid is

$$\frac{p}{} = g(z_t \quad z) + \frac{S_0^2 w_0^2}{2} \quad \frac{1}{S_z^2} \quad \frac{1}{S_0^2} \tag{85}$$

whence

$$\frac{1}{}\frac{@p}{@z} = \quad g \quad \frac{1}{2}\frac{S_0^2 u_0^2}{S^3}\frac{@S}{@z} \tag{86}$$

For a typical Dines manometer with $S \quad 0{:}01\,m^2$, $@S=@z \quad 0{:}005\,m$, the second (i.e. perturbation) term in this equation is small provided that

$$u_0^2 < \frac{2Sg}{@S=@z} \quad 40\,m^2 s^{\ 2} \tag{87}$$

As this condition is satis ed, there is no need to modify the pressure distribution calculated in the previous section to account for the presence of constrictions to the ow.

3.5 Equations for the moving system

3.5.1 Forces on the oat

The vertical component of the forces on the oat are as follows:

The force due to the difference in air pressure,

$$F_1 = \quad p\,Y(x_2) \tag{88}$$

The force due to water pressure on the bottom of the buoyancy collar,

$$\begin{aligned} F_2 &= p_{out}(y_3)(A \quad Y(x_3)) \\ &= (p_d \quad (g + \quad)y_3)(A \quad Y(x_3)) \end{aligned} \tag{89}$$

The force due to water pressure on the outside of the oat below the buoyancy collar,

$$\begin{aligned} F_3 &= \int_{x_{d0}}^{x_3} p_{out} Y'(x)\,dx \\ &= p_d f\,Y(x_3) \quad Y(x_{d0})g + (\ g \quad) \quad y_3 Y(x_3) + y_b Y(x_{d0}) \int_{x_{d0}}^{x_3} Y(x)\,dx \end{aligned} \tag{90}$$

The force due to water pressure on the inside of the oat

$$\begin{aligned} F_4 &= \int_{x_{d0}}^{x_2} p_{in} Y'(x)\,dx \\ &= \quad p_d f\,Y(x_2) \quad Y(x_{d0})g \quad (g + \quad) \quad y_2 Y(x_2) + y_b Y(x_{d0}) \int_{x_{d0}}^{x_2} Y(x)\,dx \end{aligned} \tag{91}$$

The force due to the mass of the oat

$$F_5 = \quad mg \tag{92}$$

The net force, excluding damping, is the sum $F_1 + F_2 + F_3 + F_4 + F_5$.

3.5.2 Forces on the water

The acceleration of the free surface of the water outside the oat is now derived. In the z-coordinate system of Fig 16, the equation of motion for the water is

$$\frac{@w}{@t} + w\frac{@w}{@z} = \quad \frac{1}{} + gs \tag{93}$$

wheres is the sign ofz. Assuming that the motion is uniform across the channel,

S43 3.909 T10.909 Tf 284.4 578 Td. Assumf4(t)-0eF

3.5.3 Damping

Three forms of damping are considered. The oat and water each have linear damping of their motion with time-scales $_f$ and $_w$ respectively. In addition, the relative motion of the oat and water is damped. The relative velocity of water through the choke at the bottom of the oat is

$$v_{choke} = v_b + v_1 \frac{C \quad A}{Y(x_b)} \tag{99}$$

where v_b is the velocity of the oat and v_1 is the velocity of the water level outside the oat, both relative to the tank. This ow is assumed to exert a drag force

$$C_{choke} j v_{choke} j v_{choke} \tag{100}$$

as it passes through the choke, leading to accelerations on the water and the tank of

$$C_{choke} j v_{choke} j v_{choke} = m \tag{101}$$

and

$$C_{choke} j v_{choke} j v_{choke} = (V) \tag{102}$$

respectively.

3.6 Simulations with no damping

The equations of motion of the system are solved as before, by fourth-order Runge-Kutta.

Figure 17 summarises the behaviour of the system in the absence of damping. As for the U-tube analogue, there are two dominant resonant frequencies, with the water moving in- or out-of-phase with the oat. (Some care is needed in describing these, since the water position in the oat, x_2, corresponds to the water position below the piston, which was x_1 in the notation of that section). The gure shows that the lower-frequency oscillation, in which the oat and water inside it move in phase, has a frequency of 0.49 Hz at 10 m s ^{1}, which slowly increases with wind speed to 0.57 Hz at 25 m s ^{1} and to 0.75 Hz at 50 m s ^{1}. The higher-frequency, out-of-phase motion, has a frequency that increases from about 1.3 Hz as the mean wind speed increases from 10 to 50 m s ^{1}.

At a mean wind speed of 20 m s ^{1}, similar to that of the laboratory measurements conducted by the Cyclone Testing Station, the two frequencies are about 0.55 Hz and 1.45 Hz, within about 0.1 Hz of the measured resonant frequencies. This is excellent agreement; the small discrepancy is probably mainly due to the relatively crude modelling of the motion of the water, particularly around the bottom of the tank, that damping may slightly shift the frequencies, and experimental uncertainty in the measured frequencies. The rst of these factors is considered to be the most likely, as the assumptions made about that ow determine the effective oscillating masses. If part of the water participates in the oscillation to a lesser degree — for example, that in the bottom corners of the tank — then this would reduce the oscillating mass and increase the resonant frequencies, possibly suf ciently to account for the discrepancy with observations.

As with the U-tube and piston analogue, there are also weaker spectral peaks at harmonics and interharmonics of the dominant resonances.

Modelling the Transient Response of the Dines Anemometer

The strong agreement with the laboratory measurements provides considerable confidence in the model. There is no tuning of these results, they were obtained simply by inserting the correct float geometry and mass and chamber geometry, into the equations.

In particular, the agreement validates the decision to assume that the pressure inside the tank is equal to that at the pitot tube entrance. This decision was based on calculations and measurement showing that the tubing resonance terminated into a fixed volume was about 6 Hz, much higher than the manometer resonances. As a check, a version of the model was constructed in which the mass of air inside the float was held fixed and the pressure determined through Boyle's Law, as in the U-tube analogue. This version shifted the out-of-phase oscillation to much higher frequencies, as the effective spring constant was greatly increased, somewhat similarly to the U-tube case where the external pressure was nonzero. The poor agreement with observations of this version validates the original decision about pressure.

It is worth commenting upon the “restoring force” that enables the oscillation. In the U-tube analogue, this force is the compressed or rarefied air. Here, it is that a departure of the system from equilibrium means that the effective area on which the air pressure acts on the float and the water, $Y(x$

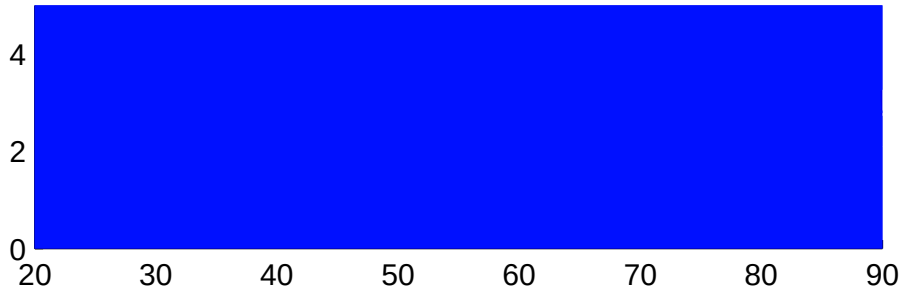
4
2
0
20
30
40
50
60
70
80
90

care will be needed in interpreting the results of this study to ensure that the appropriate model of Dines anemometer is considered. Of the three versions used, the most common were the low-speed and high-speed measured as part of Task 3, which had maximum readings of 100 and 200 miles per hour respectively. However, there was also an intermediate instrument, with a maximum reading of 150 m.p.h., no examples of which survive in Australia. It is apparent from the surviving chart that the winds in Cyclone Tracy were measured by the 150 m.p.h. instrument, and there is physical and anecdotal evidence for one having been previously installed at Learmonth. In addition, the Bureau's instrument laboratory have published test results on such an instrument. Unfortunately, more detailed documentary evidence has proved elusive.

Measurement of the characteristics of onete60Ponte60Poo6e survivily instrumein pt tDi sveiin fudenre fv

References

Borges, A. R. J., 1968: On the frequency response of floater-type anemographs (velocity fluctuations in the direction of mean speed). *Technica*, 379, 505–511.

Gold, E., 1936: Wind in Britain – The Dines anemometer and some notable records during the last 40 years. *Quart. J. Roy. Meteor. Soc.*, 62, 167–206.

Appendix III: Task 3

Experimental testing of the Dines pressure tube and float for dynamic characteristics using a rapid Pressure Loading Actuator (PLA).

John Ginger and David Henderson
Cyclone Testing Station,
James Cook University
Townsville, 4811, Australia

1 Introduction

The objective of Task 3 of the project was to measure the response of low-speed and high-speed Dines systems when excited by a known pressure signal to the Dines head (inlet pitot port). The input pressure traces and the measured outputs are to provide comparison data for Task 2. A range of pressure signals with differing frequencies and amplitudes were generated using a Pressure Loading Actuator (PLA) capable of applying rapidly fluctuating realistic wind pressures.

Figure 1 shows the 3-cup anemometer at the Bureau of Meteorology at the Townsville Airport.

Figure 1. 3-cup anemometer

Figure 2. Dines anemometer

Figure 3. High Speed Float Chamber

Figure 4. Float rod and speed recorder

2 Experimental setup and Data collection

Several configurations, isolating each component in turn; the Dines head, the float chamber and the 10 m tubing, were tested for assessing their contributions to the overall response of the instrument. The 10 m of tubing is the typical height of the head above ground level. The dynamic response of the Dines is complex and is dependent on the characteristics of the applied pressure fluctuations and the mass of the float/rod and the column of water in the chamber.

Pressure input to the Dines

Advanced real time pressure loading systems capable of high flow have been developed for WKH ³7KUHH /LWWOH 3LJV´ /3 IXOO VFDOH KRXUOH WHVWLQJ Ontario

(UWO) (Kopp et al. 2010). The pressure load actuator (PLA) is used to apply actual turbulent wind

Figure 6. Manifold and stand for connection PLA to Dines head/vane. Note the two pressure transducers located at the inlet of the Dines head.

The response of the float chamber to the applied pressure was measured using a linear variable differential transformer (LVDT) connected to the shot-cup on top of the float rod as shown in Figure 7. A small universal joint was used to connect the shot-cup to the LVDT. A crucial requirement was to ensure that the weight of the universal joint, modified shot-cup and LVDT shaft was equal to the weight of the original shot-cup, lead shot and pen.

Figure 7. LVDT measuring movement of float rod

Test configurations

A range of test configurations were set-up to examine the contribution of each component of the Dines systems to the overall frequency response. The tests included assessing the response of both the high-speed and low-speed Dines float chambers, as well as investigating the contribution of the Dines Head (with associated bends), and the connecting tubing to the overall response of the system.

The test configurations were;

1. PLA connected to 10 m PVC tube (30 mm internal diameter) with 225 mm long 100 mm internal diameter *fixed* float volume at the output end (i.e. Dines head and float chamber not used)

(a) (b)

Figure 8. (a) Fixed volume at end of 10 m pipe and (b) inlet of 10 m straight tube

A series of cyclic and other fluctuating input pressure traces were applied. The results obtained from the cyclic pressure inputs are given in Table 1, in terms of the Standard deviation and Peak output to input pressure ratios. The amplification of pressure as the cyclic frequency approaches 6 Hz is evident with the standard deviation ratio exceeding 5.0.

Table 1. Sinusoidal traces for Configuration 1

					Ratio of output over input	
Trace	Type	Freq (Hz)	Target Min (kPa)	Target Max (kPa)	Std dev ratio	Peaks ratio

Figure 12. Dines head connected to fixed float volume

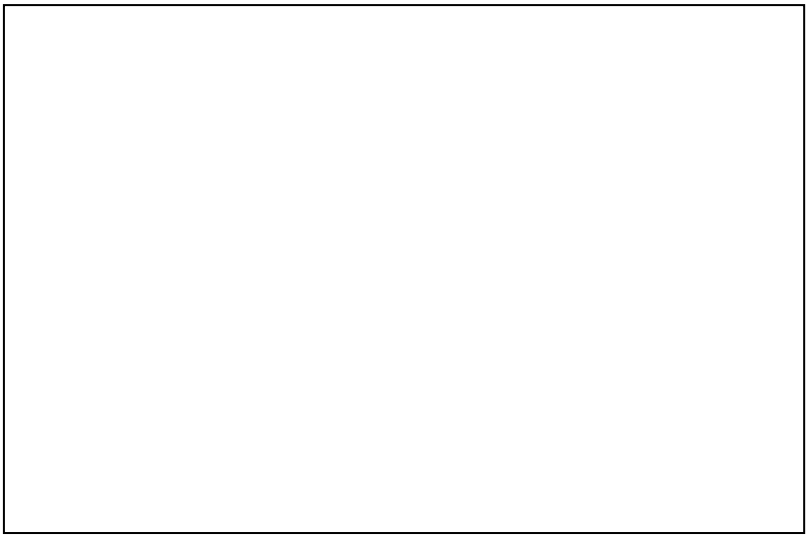

Figure 14. Output/input standard deviation ratios for sine waves two amplitude ranges ± low-speed Dines float chamber

The input and output spectra for a white-noise input pressure signal with an amplitude of 0.5 to 1.0 kPa is shown Figure 15. The output spectrum shows the characteristic double peak similar to Borges (1968).

Figure 15. White noise input of 0.5 to 1.0 kPa with output of float (LVDT)

Configuration 5

The PLA is connected to Dines head (including right angle bends) to the low-speed Dines float chamber (i.e. without 10m length of tube), and subjected to white-noise input pressure of 0.5 to 1.0kPa signal. The input and output spectra shown in Figure 16 indicates the characteristic double peak at 0.8 and 1.2 Hz. Comparing Figure 15 with Figure 16, shows that 10m tube length only effects the higher frequencies around 6 Hz. That is the 10 m tube has little influence on the Dines float response for the frequencies in the range of significant wind velocity fluctuations (< 3 Hz).

Figure 16. White noise input of 0.5 to 1.0 kPa with output of float (LVDT)

Configuration 6

The PLA is connected to Dines head (including right angle bends) and the high-speed float chamber. The tests were conducted with the Dines high-speed unit located at the Townsville airport. Figure 17 shows the test setup. A summary of these findings were presented by Henderson et al (2010)

Figure 17. PLA (in utility) connected to volume chamber which is connected to high-speed Dines

Cyclic (i.e. sinusoidal) input pressure traces generated float responses that reflected its spectrum to white noise. The displacement of the float was dependent on the magnitude of the pressure range and the frequency. Figures 19 and 20 show the response of the High speed Dines unit to a range of Sinusoidal pressure traces. The attenuation of the pressure signals at approximately 0.8 Hz and the change in phase at 1.3 Hz is evident.

Figures 21 to 24 show the response of the high-speed Dines unit to a range of square wave pressure traces of amplitudes 0 to 3 kPa and periods from 10 seconds to 2.5 seconds. The GLVWLQFW ³NLQN´ DQG WKH RYHUVKRRW LQ EDWWH UHVSRQVH can with the low-speed Dines. The time taken for the LVDT to settle depends on the amplitude.

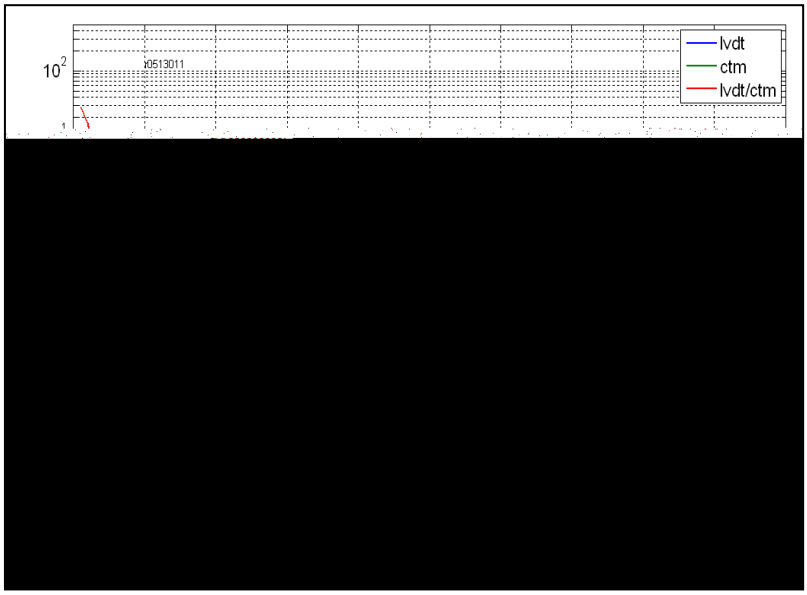

Figure 18. White-noise spectrum (mean 1 kPa, max 1.5 kPa)

Figure 19. Input sine pressure 0.8 Hz, 1 to 3 kPa showing attenuation of Dines output

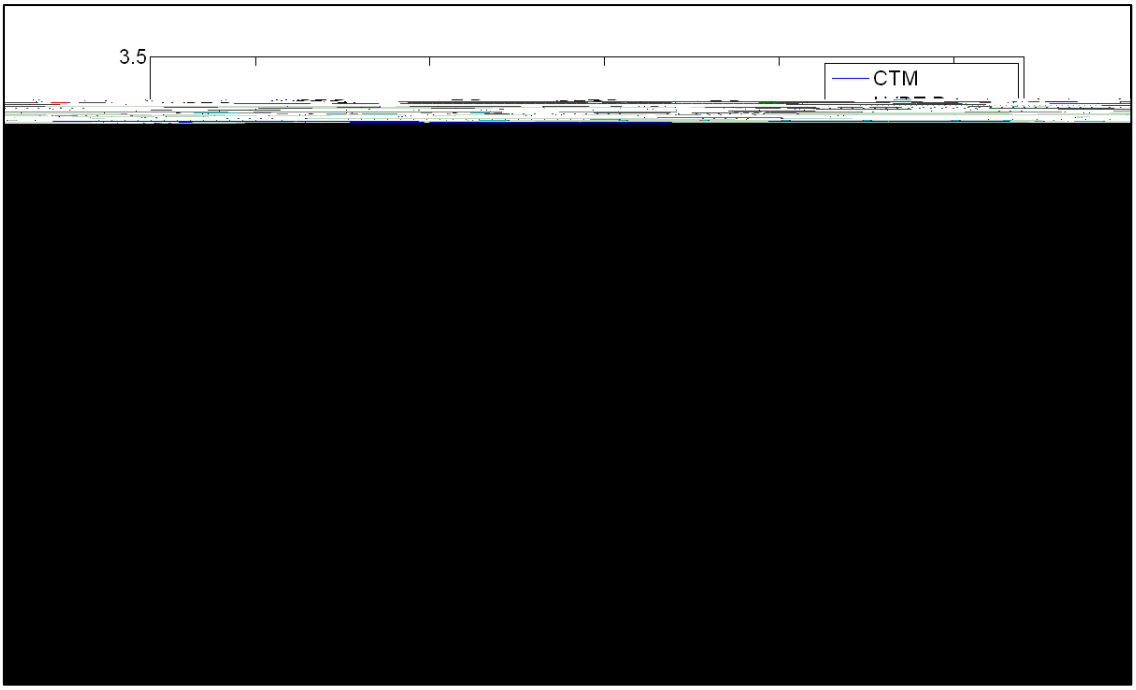

Figure 22. Input square wave pressure 1.5 kPa amplitude with period of 10s

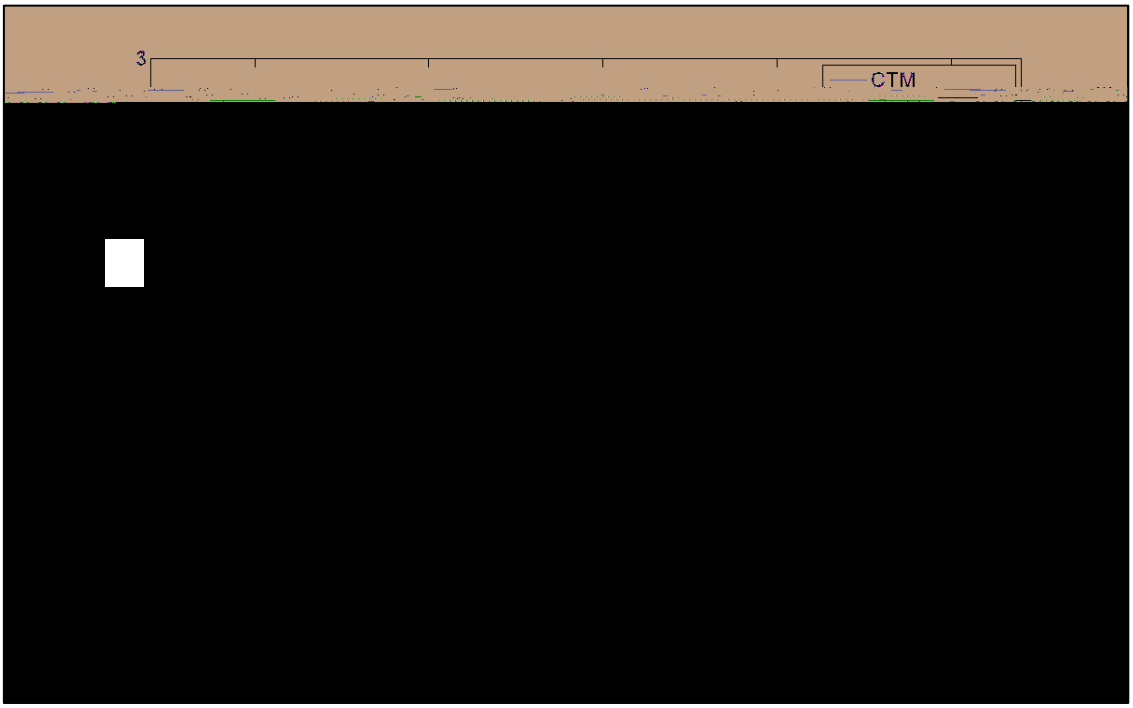

Figure 23. Input square wave pressure 0.75 kPa amplitude with period of 10s

Figure 24. Input square wave pressure 1.5 kPa amplitude with period of 5 seconds

The high-speed Dines was V X E M H F W H G W R D U D Q J H R I ³V L P X O D W H G L
measured wind velocity traces. The mean value of the output pressure (measured using the time averaged mean displacement of the LVDT) matched the mean input pressure. Figure 25 shows a 30sec portion of input wind pressure derived from a measure10(a)-a ed ched79(su)9(r)-3(e)5(2)-(at)-5(ch0(1(ed7-4(g

Figure 25. Portion of wind trace with 1s moving averaged filter on input pressure traces of CTM and PLA and the output of the LVDT converted to pressure

4 Discussion

The low-speed and high-speed Dines instruments were calibrated for their mean (time averaged) response to static pressures (i.e. steady velocity). The static pressure test provided a calibration factor that relates the vertical displacement of the float rod (in mm) to the applied pressure difference (in Pa) which is converted to the velocity in m/s. The calibration factors obtained are used in the series of fluctuating pressure tests (i.e. sinusoidal, square waves, white noise and pressure signals representing actual velocity), to determine their dynamic response.

ed e<lacet-18.6 Td()ca ure

Figure 26. Wind speed converted from applied PLA pressure vs vertical displacement of float rod (measured by LVDT) ±Low Speed Dines

Figure 27. Wind speed converted from applied PLA pressure vs vertical displacement of float rod (measured by LVDT) ±

Test data file structure and description provided to project partners for Stage 2

Tests of PLA with PVC tube network (in CTS lab space)

PLA connected to 10 m PVC tube (30 mm internal diameter) with 225 mm long 100 mm internal diameter fixed float volume at end (i.e. NOT using Dines head or float chamber)

IRLBH2010DJHDines\dcc_pt\Test_Data\IRLBH20100427005	27-r5	27/04/2010	sine	0.3 hz at 1 to 3 kPa
IRLBH2010DJHDines\dcc_pt\Test_Data\IRLBH20100427028	27-r28	27/04/2010	sine	0.2 hz at 1.8 to 2.2 kPa
IRLBH2010DJHDines\dcc_pt\Test_Data\IRLBH20100427029	27-r29	27/04/2010	sine	6 hz at 1.8 to 2.2 kPa
IRLBH2010DJHDines\dcc_pt\Test_Data\IRLBH20100427030	27-r30	27/04/2010	sine	2 hz at 1 to 3 kPa
IRLBH2010DJHDines\dcc_pt\Test_Data\IRLBH20100427031	27-r31	27/04/2010	dynamic	white noise
IRLBH2010DJHDines\dcc_pt\Test_Data\IRLBH20100427032	27-r32	27/04/2010	sine	1 hz at 1 to 3 kPa
IRLBH2010DJHDines\				

_Data\IRLBH20100504005

Tests at Bureau (airport)

PLA connected to Glenlitta Dines head (incl right angle bends) to high-speed float chamber

IRLBH2010DJHBOM\float_ctm_lvdt\Test_Data\IRLBH20100512006	12r6	40310	sine	0.2 hz at 1 to 3 kPa
IRLBH2010DJHBOM\float_ctm_lvdt\Test_Data\IRLBH20100512007	12r7	12/05/2010	dynamic	TTU_JDG
IRLBH2010DJHBOM\float_ctm_lvdt\Test_Data\IRLBH20100512008	12r8	12/05/2010	step	Step trace
IRLBH2010DJHBOM\float_ctm_lvdt\Test_Data\IRLBH20100512009	12r9	12/05/2010	sine	0.2 hz at 1.8 to 2.2 kPa
IRLBH2010DJHBOM\float_ctm_lvdt\Test_Data\IRLBH20100512011	12r11	12/05/2010	dynamic	white noise 1 kPa mean
IRLBH2010DJHBOM\float_ctm_lvdt\Test_Data\IRLBH20100512012	12r12	12/05/2010	sine	1 hz at 1 to oa/33q9.96 Tf796

Tests on Low speed Dines (in CTS lab space)

PLA connected to Dines head (incl right angle bends) to 10 m PVC tube (30 mm internal diameter) with Dines low-speed float chamber at end

IRLBH2010DJHlowspeed\float_ctm_lvdt\Test_Data\IRLBH20100521005	21r5	21/05/2010	step	Step trace
IRLBH2010DJHlowspeed	21r6	21/05/2010	dynamic	white noise
IRLBH2010DJHlowspeed	21r9	21/05/2010	dynamic	TTU_JDG
IRLBH2010DJHlowspeed\float_ctm_lvdt\Test_Data\IRLBH20100524001	24r1	24/05/2010	step	Step trace
IRLBH2010DJHlowspeed	24r2	24/05/2010	dynamic	white noise
IRLBH2010DJHlowspeed\float_ctm_lvdt\Test_Data\IRLBH20100527001	27r1	27/05/2010		

IRLBH2010DJHDines_lowspeed_jun\float_ctm_lvdt\Test_Data\etc	7r4	7/06/2010	dynamic	white noise 0.2 to 0.7 kPa
IRLBH2010DJHDines_lowspeed_jun\float_ctm_lvdt\Test_Data\etc	7r5	7/06/2010	dynamic	white noise 0.4 to 0.9 kPa
IRLBH2010DJHDines_lowspeed_jun\float_ctm_lvdt\Test_Data\etc	7r6	7/06/2010	dynamic	white noise 0.6 to 1.1 kPa
IRLBH2010DJHDines_lowspeed_jun\float_ctm_lvdt\Test_Data\etc	7r7	7/06/2010	dynamic	white noise 0.5 to 1.0 kPa
IRLBH2010DJHDines_lowspeed_jun\float_ctm_lvdt\Test_Data\etc	7r8	7/06/2010	dynamic	JK_sonic
IRLBH2010DJHDines_lowspeed_jun\float_ctm_lvdt\Test_Data\etc	7r9	7/06/2010	dynamic	white noise 0.5 to 1.0 kPa
IRLBH2010DJHDines_lowspeed_jun\float_ctm_lvdt\Test_Data\etc	7r10	7/06/2010	dynamic	white noise 0.5 to 1.0 kPa

PLA connected to Dines head (incl right angle bends) to Dines low-speed float chamber (i.e. no 10 m pipe)

IRLBH2010DJHlowspeed_nopipe\float_ctm_lvdt\Test_Data\IRLBH20100528001	28r1	28/05/2010	dynamic	white noise 0.5 to 1.0 kPa
IRLBH2010DJHlowspeed_nopipe\	28r2	28/05/2010	dynamic	white noise 0.5 to 1.0 kPa